11176-H087-RO-00

LM AND CSM S-BAND ANTENNA TRACKING STUDIES
TASK E-53C-1
TECHNICAL REPORT

ELECTRONICS ASSEMBLY INTERCHANGEABILITY STUDY
VOLUME I
SMALL SIGNAL ANALYSIS

---

13 DECEMBER 1968

Prepared For

NATIONAL AERONAUTICS AND SPACE ADMINISTRATION
MANNED SPACECRAFT CENTER
HOUSTON, TEXAS

Under

Contract No. NAS 9-8166

TRW SYSTEMS GROUP

NASA CR 92499

11176-H087-RO-00

LM AND CSM S-BAND ANTENNA TRACKING STUDIES

ELECTRONICS ASSEMBLY INTERCHANGEABILITY STUDY
VOLUME I
SMALL SIGNAL ANALYSIS

TASK E-53C-1

Prepared by
L. H. Robinson, Jr.

13 DECEMBER 1968

Approved: ______________________
J. W. Pool, Manager
Task E-53C-1

Approved: ______________________
C. E. Blakely, Head
Sensor Systems Section

Approved: ______________________
J. DeVillier, Manager
Communication and Sensor
Systems Department

TRW
SYSTEMS GROUP

PRECEDING PAGE BLANK NOT FILMED

TABLE OF CONTENTS

TABLES

ILLUSTRATIONS

ILLUSTRATIONS (Cont'd)

ILLUSTRATIONS (Cont'd)

1.0 INTRODUCTION

As noted in Reference 1, the CSM High Gain Antenna Tracking System Interchangeability Study is intended to assure satisfactory operation of the overall tracking system when separately-tested system elements are interconnected.

1.1 GENERAL CONTENT DESCRIPTION

This report, consisting of Volumes I and II, describes the portion of the Interchangeability Study concerning the Electronics Assembly (see paragraph 2.2 of Volume I). Volume I describes the linear, small signal characteristics of the Electronics Assembly at the system level and estimates the nominal and worst-case limits of the small signal Electronics Assembly input/output transfer functions. These estimates are based on parameter data supplied by Autonetics (Reference 2). Volume II describes the Electronics Assembly switching logic functions at the equivalent circuit level and estimates the nominal and worst-case limits of the analog threshold functions. Volume II also reduces the overall switching functions to equivalent Boolean logic equations and describes typical operational sequences of events.

1.2 LINEARITY ASSUMPTION

The analyses presented in Volumes I and II are based on a <u>linear</u> model of the CSM High Gain Antenna Tracking System, where saturation and other non-linearities have been neglected. Thus, the results presented are valid only for small tracking errors, up to about ± 0.1 degrees or less.

1.3 VOLUME I CONTENT DESCRIPTION

Volume I focuses attention on the small signal characteristics of the Electronics Assembly. It presents formulas and curves that relate the output servo motor drive voltages to the input receiver AGC error voltage and the tachometer rate-feedback voltages. As such, it assumes that linear, small signal approximations are valid, that there is no excessive tracking error (less than $\pm 1°$) (i.e., the system is in the narrow-beam, high-gain tracking mode), that there is no scan limit approach (scan limit warning) or scan limit effects, and that there is no whiparound.

Section 2.0 describes the tracking system in enough detail to introduce important operating characteristics and parameters. Section 3.0 models the small signal Electronics Assembly and develops general input/output equations. Section 4.0 gives tabulated and plotted results of nominal and worst-case parameter substitutions into the equations of Section 3.0. Section 5.0 presents the Volume I summary and conclusions.

2.0 SYSTEM DESCRIPTION

The CSM High Gain Antenna Tracking System keeps the CSM S-band High Gain communication antenna pointed at th. MSFN ground station by seeking-out the strongest up-link signal. As the spacecraft maneuvers, the tracking system senses the resulting pointing error and drives the antenna until the pointing error is zero.

2.1 ANTENNA GIMBALLING SYSTEM

The High Gain Antenna (HGA) is gimballed about three mutually perpendicular axes, as shown schematically in Figure 2-1. The A Axis (Gimbal 1) rotates with angle α with respect to the CSM vehicle (y_b), the B Axis (Gimbal 2) rotates with angle β relative to Gimbal 1 (x_1), and the C Axis (Gimbal 3) rotates with angle γ relative to Gimbal 2 (x_2). Note that Figure 2-1 is drawn with $\alpha = \beta = \gamma = 0$, where the antenna boresight pointing direction (the antenna $+x_3$ axis) is directly off the end of the boom. The dashed line in Figure 2-1 indicates the antenna $+x_3$ axis pointing direction for $\alpha = 0$, $\beta = 0$, and $\gamma = 90°$. This direction, being parallel to the CSM +X axis, corresponds to zero settings of the antenna Manual Positioning Pitch and Yaw controls (located in the CM).

2.2 TRACKING SYSTEM BLOCK DIAGRAM DESCRIPTIONS

Figures 2-2, 2-3, and 2-4 present various levels of block diagrams for the HGA Tracking System. The first-level block diagram Figure 2-2 shows the tracking system divided into four major sub-assemblies (Antenna Assembly, Transponder, Electronics Assembly, and Manual Control Assembly) which are interconnected at four interfaces (A, B, C, and D)*.

The Antenna Assembly is driven by a radio frequency (RF) source (the earth station up-link signal) and, at Interface C, by the servo motor drive output voltages of the Electronics Assembly. Other inputs to the Antenna Assembly via Interface C are command resolver outputs from the Manual Control Assembly (via Interface D). The Antenna Assembly

* Note that Interfaces C and D represent signal flow in both directions, while Interfaces A and B represent signal flow in one direction only.

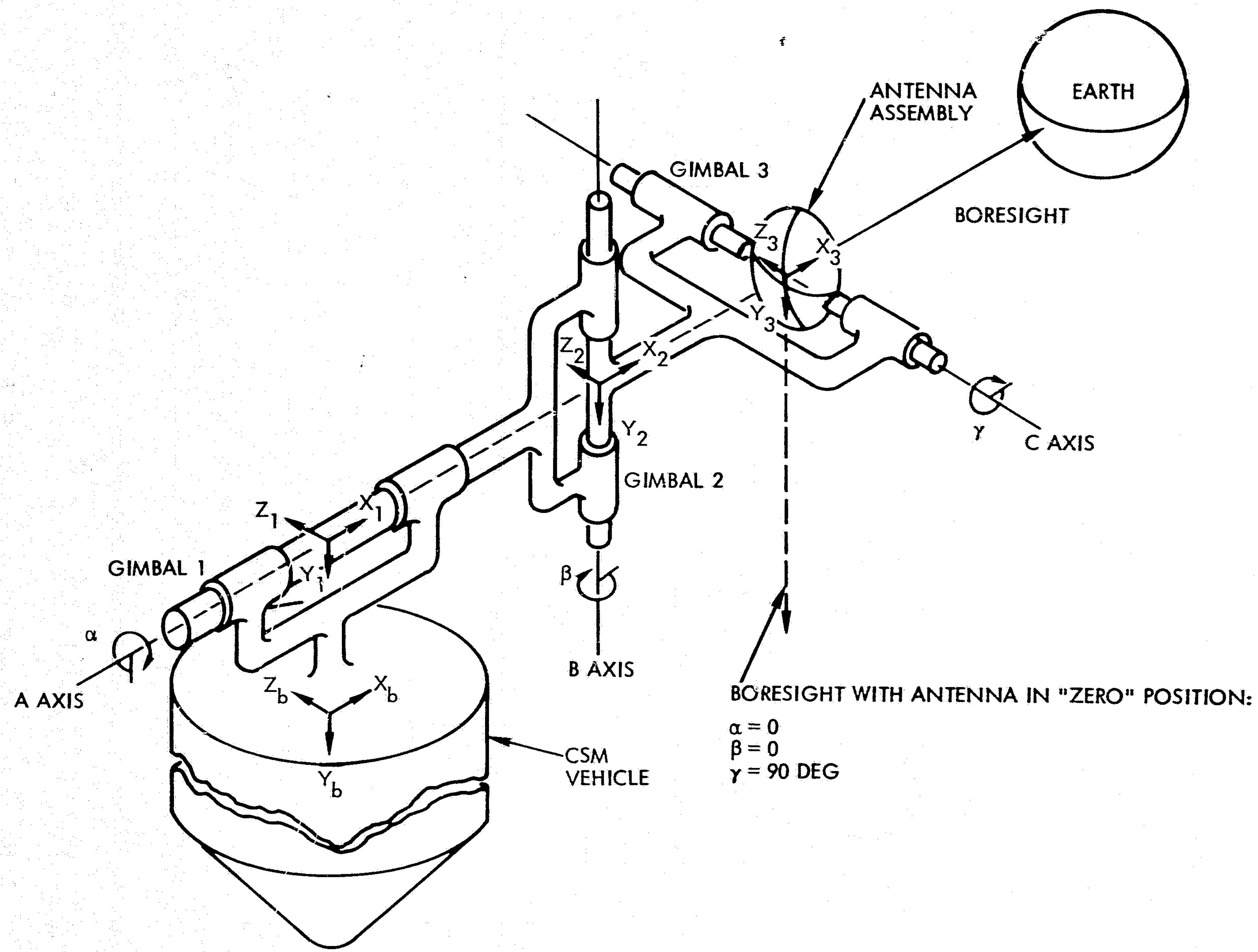

CSM High Gain Antenna Gimballing System

Figure 2-1

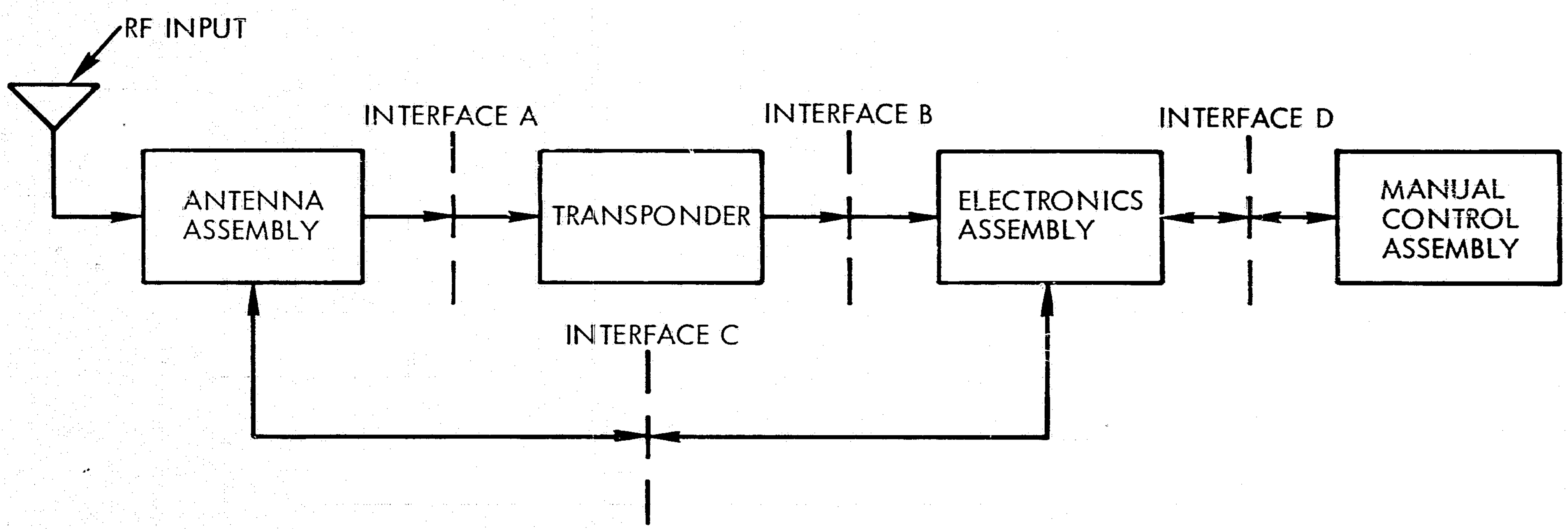

First-Level Block Diagram
CSM High Gain Antenna Tracking System

Figure 2-2

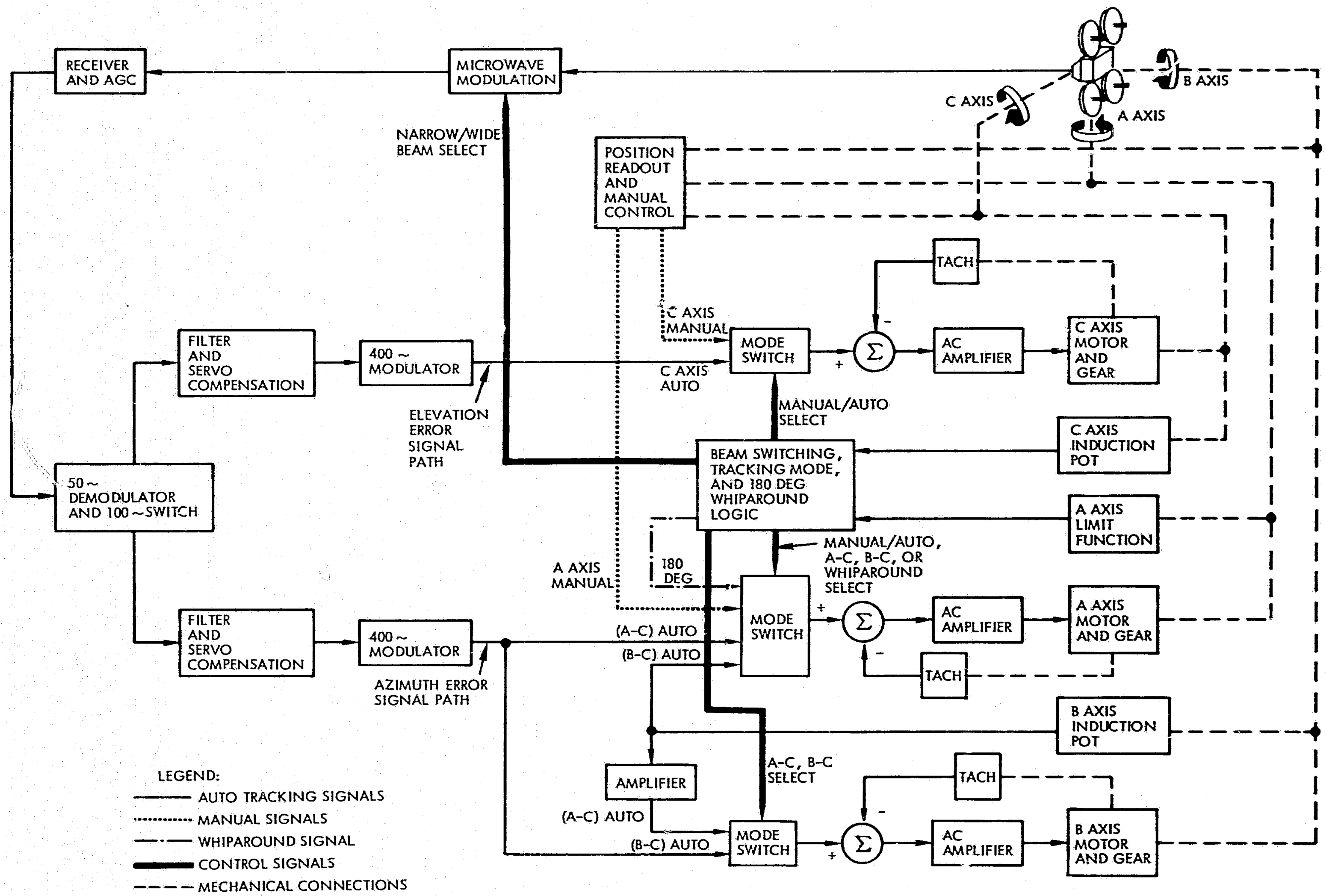

CSM S-Band High Gain Antenna Tracking System
Simplified Functional Block Diagram

Figure 2-3

FOR

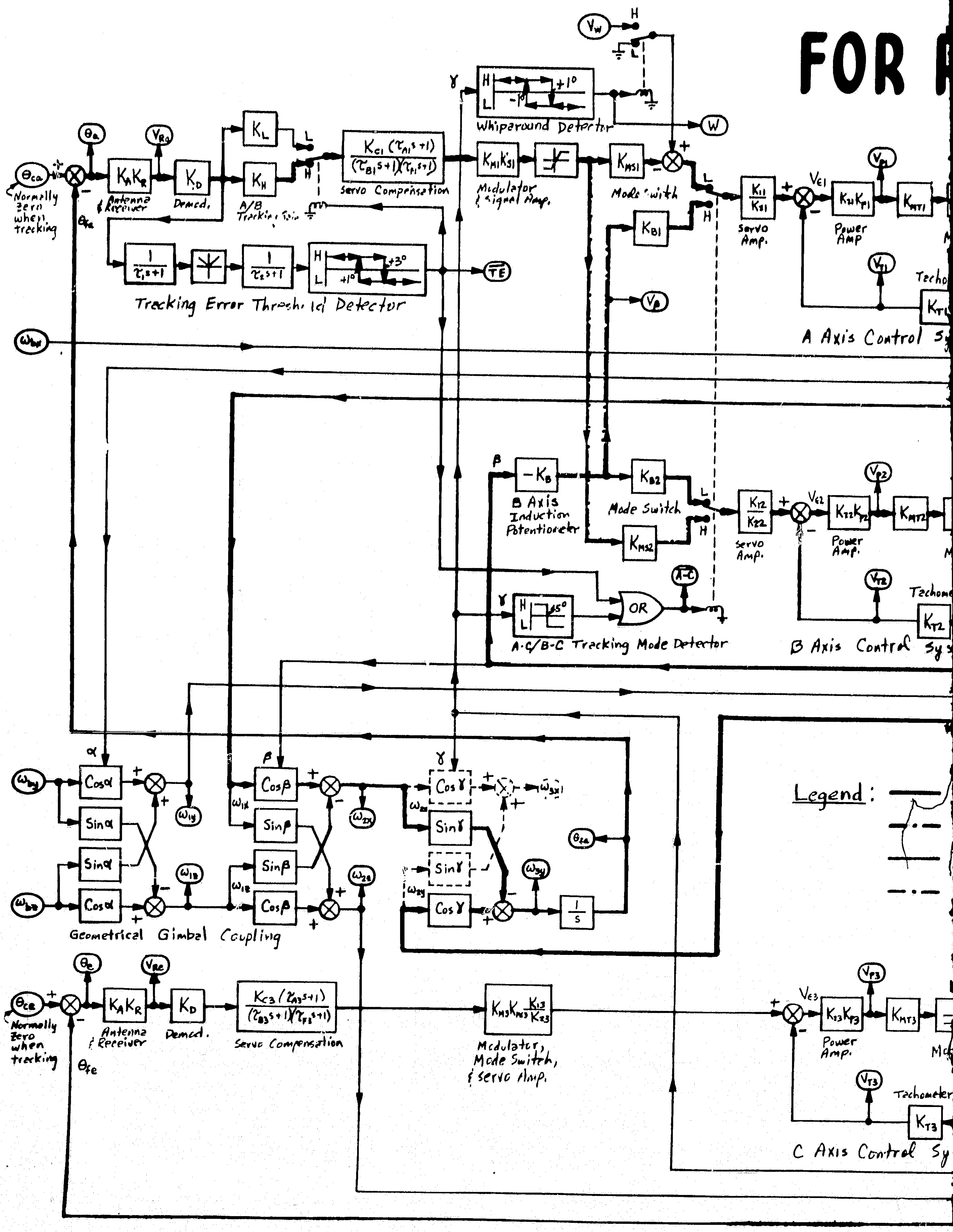

Whiparound Detector
Servo Compensation
Modulator & Signal Amp.
Mode Switch
Normally zero when tracking
Antenna & Receiver
Demod.
A/B Tracking Gain
Tracking Error Threshold Detector
Servo Amp.
Power Amp
A Axis Control Sy
B Axis Induction Potentiometer
Mode Switch
A-C/B-C Tracking Mode Detector
OR
B Axis Control Sys
Geometrical Gimbal Coupling
Legend:
Modulator, Mode Switch, & Servo Amp.
Power Amp.
Tachometer
C Axis Control Sy

2-5A

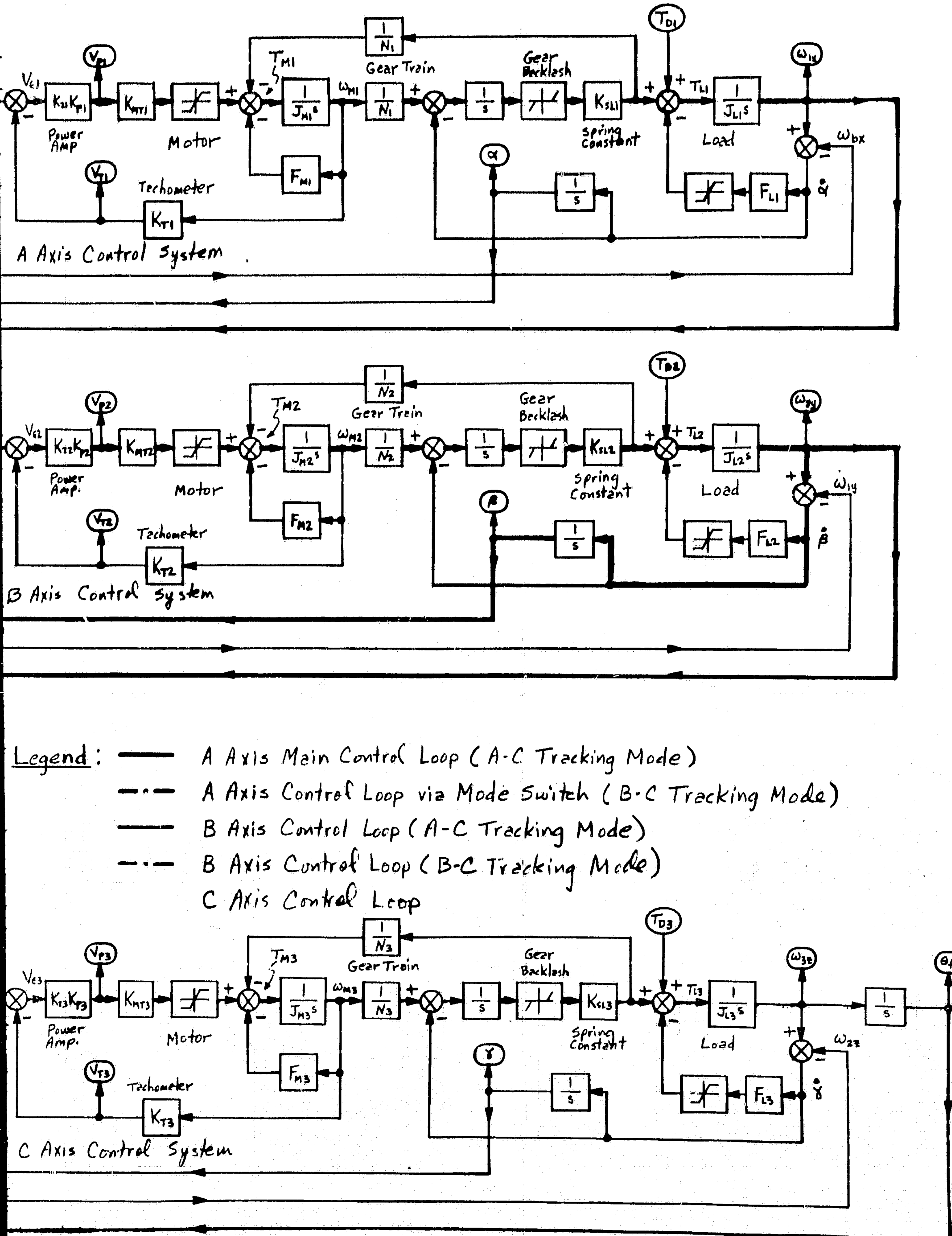

CSM High Gain Antenna Tracking System - Equivalent Functional Block Diagram

Figure 2-4

output at Interface A is an amplitude modulated (AM) carrier, whose %AM is proportional to the tracking error. The Antenna Assembly outputs at Interface C are the A, B, and C Axis Tachometer outputs, A Axis Function Generator (AFG) output, and B and C Axis Induction Potentiometer (BIP and CIP) outputs, as well as command resolver and readout resolver outputs. (See Figure 1-1, p. 1-4 of Reference 3 for a more detailed diagram at this level.)

The Transponder (receiver) is driven by the Antenna Assembly at Interface A. The Transponder converts the %AM signal to an automatic gain control (AGC) voltage proportional to the tracking error (Interface B).

In the AUTO (tracking) mode, the Electronics Assembly converts the Transponder AGC error voltage (Interface B) into servo motor drive voltages (Interface C). In the MAN (manual) mode, the Electronics Assembly converts the Antenna Assembly command resolver outputs (Interface C) into servo motor drive voltages (Interface C). In either mode, the servo motor drive voltages are influenced by the Antenna Assembly tachometer feedback voltages (Interface C). The system operates to reduce the error voltages to zero.

The Manual Control Assembly transmits command resolver signals to, and receives readout resolver signals from, the Antenna Assembly indirectly through the Electronics Assembly via Interfaces C and D. The command resolver signals are derived from the CM Manual Positioning Pitch and Yaw control settings, and the readout resolver outputs drive the CM Pitch and Yaw readout displays.

The important fact to remember is that, in the AUTO mode, the tracking system is operating on the Transponder AGC error voltage and thus minimizes tracking error between the antenna boresight pointing direction and the up-link signal. In the MAN mode, the tracking system is operating on an error signal which is the difference between Manual Pitch and Yaw control settings and the actual antenna position; thus, in the MAN mode, the tracking system minimizes the manual positioning error.

Figure 2-3 shows a simplified functional block diagram of the HGA Tracking System. It shows that the Antenna Assembly consists of an antenna array, a microwave modulation network, and motors, tachometers, gear trains, induction potentiometers, function generators, and resolvers for the A, B, and C Axes. The Transponder contains a receiver and AGC circuit. The Electronics Assembly contains a demodulator, filter and servo compensation networks, modulators, mode switches, amplifiers, and switching logic networks. And the Manual Control Assembly consists of resolvers and displays associated with manually positioning the antenna.

A more detailed, equivalent functional block diagram of the HGA Tracking System is shown in Figure 2-4. This diagram includes only those items pertinent to the AUTO tracking mode.* An associated list of parameter values is given in Table 2-1.** Since Figure 2-4 is inaccurate in several details, it is marked "For Reference Only" and is not intended for general use. A more complete, corrected figure will appear in a later report on the dynamic tracking behavior of the CSM HGA Tracking System.

Referring to Figures 2-1, 2-3, and 2-4, the operation of the HGA Tracking System can be briefly summarized as follows:

The antenna boresight pointing error can be separated into two orthogonal components: the Azimuth error is measured about the antenna y_3 axis, while the Elevation error is measured about the antenna z_3 axis. Rotations about the antenna boresight $+x_3$ axis do not contribute to pointing errors.

Tracking errors are sensed in the antenna array and microwave modulation network, which sequentially adds the resulting azimuth and elevation error signals to the received carrier signal in the form of amplitude modulation. This modulation, denoted by K_A in Figure 2-4 and Table 2-1, represents the tracking error as %AM/deg.

The time-multiplexed azimuth and elevation errors are processed in the Transponder, which produces an AGC voltage proportional to the %AM

* Other modes are described in Volume II of this report.

** Table 2-1 is more up to date than Figure 2-4, so there may not be a one-to-one correspondence between the two.

Parameter Name	Parameter Symbol	Units	Temp °F	A Axis HI	A Axis NOM	A Axis LO	B Axis HI	B Axis NOM	B Axis LO	C Axis HI	C Axis NOM	C Axis LO
Antenna Modulation Index	K_A	%AM/Deg	77 & 200	2.70	2.25	1.80	→	→	→	→	→	→
Receiver Gain	K_R	Vrms/%AM	77 & 200	0.60	0.50	0.40	→	→	→	→	→	→
Demodulator Gain	K_D	V/Vrms	77 200	0.89 0.89	0.86 0.86	0.84 0.83	→ →	→ →	→ →	→ →	→ →	→ →
Tracking Error Compensation Gain	K_{TE}	Deg/V	77 & 200	1.10	1.00	0.90	—	—	—	—	—	—
Tracking Error Compensation (τ_1, τ_2)	$G_{TE}(s)$	V/V	77 & 200		$\frac{1}{(0.23s + 1)(0.11s + 1)}$		—	—	—	—	—	—
Azimuth Channel Low Gain	K_L	V/V	77 & 200		0.10		—	—	—	—	—	—
Azimuth Channel High Gain	K_H	V/V	77 & 200		1.00		—	—	—	—	—	—
Servo Compensation Gain	K_C	V/V	77 200	2.62 2.64	2.56 2.56	2.50 2.49	→ →	→ →	→ →	2.41 2.42	2.35 2.35	2.29 2.28
Servo Compensation Limit	K_C'	V	77 200		0.35 0			→ →		—	—	—
Servo Compensation (τ_A, τ_B, τ_F)	$G_C(s)$	V/V	77 & 200		$\frac{(0.234s + 1)}{(0.015s + 1)(1.22s + 1)}$			→			$\frac{(0.166s + 1)}{(0.0125s + 1)(0.833s + 1)}$	
Modulator Gain	K_M	Vrms/V	77 200	1.76 1.77	1.74 1.74	1.725 1.71	→ →	→ →	→ →	0.570	0.546 0.483	0.468 0.463
Modulator Phase Shift	ϕK_M	Deg	77 200	49	34	26	→	→	→	16	25 25.5	40 20
Signal Amp. Gain	K_S	Vrms/Vrms	77 & 200	0.78	0.75	0.725	→	→	→	—	—	—
Signal Amp. Saturation Limit	K_S'	Vrms	77 & 200		5			→		—	—	—
Mode Switch Gain	K_{MS}	Vrms/Vrms	77 200	0.924	0.908	0.895	0.443 0.413	0.410 0.390	0.376 0.355	1.0	1.0	1.0
Mode Switch Phase Shift	ϕK_{MS}	Deg	77 200	-1 -6	-4.3 -9	- 7 -12	-2.9 0	-5.7 -5.7	- 8.6 -11.5	0	0	0
Servo Amp. Gain Ratio	K_1/K_2	Vrms/Vrms	77 & 200	2.035	1.965	1.895	8.74	8.45	8.15	8.74	8.45	8.15
Tachometer Gain	K_T	Vrms/Deg/Sec	77 & 200	$10.0x10^{-5}$	$8.34x10^{-5}$	$6.67x10^{-5}$	$10.0x10^{-5}$	$8.34x10^{-5}$	$6.67x10^{-5}$	$10.0x10^{-5}$	$8.34x10^{-5}$	$6.67x10^{-5}$
Tachometer Phase Shift	ϕK_T	Deg	77 & 200	25	0	-25	25	0	-25	25	0	-25
Servo Amp./Power Amp. Gain Product	K_2K_P	Vrms/Vrms	77 200	168 164	137 131	92 91.5	86 84	70 67	47 46.7	86 84	70 67	47 46.7
Power Amp. Phase Shift	ϕK_P	Deg	77 200	13.7 39.5	15.1 43.2	14.4 43.9	13.7 39.5	15.1 43.2	14.4 43.9	13.7 39.5	15.1 43.2	14.4 43.9
Motor-Torque Gain	K_{MT}	in-oz/Vrms	77 & 200		0.0111			0.0111			0.0111	
Motor-Torque Limit	K_{MT}'	in-oz	77 & 200		0.4			0.4			0.4	
B Axis Ind. Pot. Gain	K_B	Vrms/Deg Vrms/Rad	77 & 200	—	—	—	0.12 6.84	0.10 5.70	0.08 4.56	—	—	—

Motor-Torque Gain	K_{MT}	in-oz/Vrms	77 & 200	0.0111			0.0111			0.0111		
Motor-Torque Limit	K'_{MT}	in-oz	77 & 200	0.4			0.4			0.4		
B Axis Ind. Pot. Gain	K_B	Vrms/Deg Vrms/Rad	77 & 200	———			0.12 6.84	0.10 5.70	0.08 4.56	———		
A Axis BIP Mode Switch Gain	K_{B1}	Vrms/Vrms	77 200	0.924 0.924	0.908 0.908	0.895 0.895	———			———		
A Axis BIP Mode Switch Phase Shift	ϕK_{B1}	Deg	77 200	-1 -6	-4.3 -9	- 7 -12	———			———		
B Axis BIP Mode Switch Gain	K_{B2}	Vrms/Vrms	77 200	———			1.61 1.79	1.43 1.59	1.19 1.03	———		
B Axis BIP Mode Switch Phase Shift	ϕK_{B2}	Deg	77 200	———			-6 0	-20.5 - 8.6	-33 -33	———		
Motor Inertia	J_M*	in-oz-sec²	77 & 200	31.9×10^{-6}			31.9×10^{-6}			31.9×10^{-6}		
Motor Static-Friction Limit	F_{MS}	in-oz										
Motor Coulomb-Friction Limit	F_{MC}	in-oz										
Motor Viscous-Friction Constant	F_{MV}	in-oz/Deg/Sec	77 & 200	0.925×10^{-5}			0.925×10^{-5}			0.925×10^{-5}		
Motor/Load Gear Turns Ratio	N	———	77 & 200	1000			2000			3000		
Gear Backlash	θ_{BL}	Deg	77 & 200	0.172	0.0573		0.172	0.0573		0.172	0.0573	
Load Spring-Constant	K_{SL}	in-oz/Deg	77 & 200	2.2×10^4			2.8×10^4			2.8×10^4		
Load Inertia	J_L*	in-oz-sec²	77 & 200	380			290			287		
Load Static-Friction Limit	F_{LS}	in-oz	77 & 200	100	50	25	200	100	50	300	150	75
Load Coulomb-Friction Limit	F_{LC}	in-oz	77 & 200	100	50	25	200	100	50	300	150	75
Load Viscous-Friction Constant	F_{LV}	in-oz/Deg/Sec	77 & 200	4	2	1	8	4	2	12	6	3

→ Means Common Circuitry (numbers are carried over)
——— Means Parameters are not in indicated axes
Blank Means no value specified
* Consistent units for inertias J_M and J_L are in-oz/Deg/Sec², so the factors given in this table for J_M and J_L should either be divided by 180 Deg/πRad = 57.296 Deg/Rad or multiplied by πRad/180 Deg = 0.017453 Rad/Deg.

CSM HGA Tracking System Parameter Values

Table 2-1

on the received carrier signal. This receiver transformation is represented by K_R (vrms/%AM). The receiver output (actually a 100 Hz time-multiplexing of the signals V_{Ra} and V_{Re} in Figure 2-4) is effectively $K_A K_R$ vrms/deg.

The receiver output AGC signal is processed by a 50 Hz demodulator and 100 Hz switch, represented by K_D, which separates the multiplexed azimuth and elevation signals into separate channels. The demodulated outputs are dc voltages which are proportional to the azimuth and elevation errors, respectively. The demodulator outputs are processed by active "servo compensation" networks, represented by K_C and $G_C(s)$*, which insert lead-lag poles and zeros into the system transfer functions.

The compensated azimuth and elevation error dc signals are converted into 400 Hz ac signals by modulators, represented by K_M, which introduce phase shifts ϕ_{K_M}.** The 400 Hz modulator outputs are gated into the remainder of the A, B, and C Axis control systems via mode switches***, represented by K_{MS} (and K_{B1} and K_{B2}), which insert phase shifts $\phi_{K_{MS}}$ (and $\phi_{K_{B1}}$ and $\phi_{K_{B2}}$). In addition to providing the AUTO track connections shown in Figure 2-4, the mode switches also provide the switchpoints for the Manual Mode and Inhibit Function; neither of these latter functions is included in this description and are contained in Volume II of this report.

---

* Note that the final subscripts 1, 2, and 3 refer to the A, B, and C Axes, respectively.
Also note that the tracking error threshold detector inserts either a high or low gain (K_H or K_L) into the azimuth channel, depending on whether the absolute value of the tracking error is above or below a threshold. This detector also controls which antenna array is used, the wide-beam for excessive tracking errors and the narrow-beam for small tracking errors. Further discussion of this operation is contained in Volume II of this report. The diode limiting in $G_{C1}(s)$ is not shown in Figure 2-4.

** Ideally, positive errors are represented by amplitude-modulated 400 Hz, +90° phase shift signals, and negative errors are represented by amplitude-modulated 400 Hz, -90° phase shift signals. The modulator phase shift ϕ_{K_M} is added to the +90° and -90°, respectively. The ϕ's are not shown in Figure 2-4.

*** The azimuth channel also has a signal amplifier K_{S1} between the modulator and mode switches, whose output is limited to $\pm K'_{S1}$.

The azimuth channel modulator output is connected either to the A Axis Control System via K_{MS1} or to the B Axis Control System via K_{MS2}, depending on whether the C Axis Gimbal angle γ is greater or less than 45°: If $\gamma < 45°$, the tracking mode detector is in its "H" state, and the azimuth error signal is processed by the B Axis Control System; this condition is known as the "B-C" tracking mode. If $\gamma > 45°$, the tracking mode detector is in its "L" state, and the azimuth error is processed by the A Axis Control System; this condition is known as the "A-C" tracking mode. If the tracking error threshold detector is in its "L" state (excessive tracking error), the azimuth error is processed by the A Axis Control System, regardless of the value of γ; thus, wide-beam acquisitions always occur in the "A-C" mode. In addition, if $\gamma \leq -1°$, the whiparound detector inserts a whiparound voltage (V_W) into the A Axis Control System, causing the A Axis Gimbal to slew about 180°.

When the azimuth error signal is being fed into either the A or B Axis, the B Axis Gimbal angle β is being fed (inverted) into the other axis via K_{B1} or K_{B2}. Either mode assures that β will be near zero except during transients.

The mode switch outputs are summed with thc A, B, and C Axis Tachometer (K_T)* outputs in servo amplifiers, represented by K_1 and K_2. These servo summing amplifiers drive power amplifiers (K_P), which insert phase shifts ϕ_{K_P}. The power amplifiers close the rate loops by driving the gimbal drive servo motors, represented by K_{MT}, J_M, and F_M. The servo motors drive gear trains (turns ratio N) and tachometers (K_T), whose inverted outputs provide rate-feedback compensation signals for the summing amplifiers.

The gear trains drive torsional shafts (K_{SL}), whose torque outputs drive the gimbal loads (J_L and F_L) and are reflected back through the gear trains to the motors. The motion of the gimbals is, of course, the controlled variable of the HGA Tracking System.

The remainder of Figure 2-4 consists of Sine and Cosine factors, which represent the geometrical coupling of the CSM spacecraft motion (angular velocity $\vec{\omega}_b$) to the A Axis ($\vec{\omega}_1$), of the A Axis to the B Axis ($\vec{\omega}_2$), and of the B Axis to the C Axis ($\vec{\omega}_3$). The ω_{3x} blocks are shown dashed in Figure 2-4, since they do not directly contribute to system behavior.

* The tachometers introduce phase shifts ϕ_{K_T}.

3.0 SMALL SIGNAL ELECTRONICS ASSEMBLY

Section 2.0 presented the HGA Tracking System at three different block diagram levels: the first-level block diagram (Figure 2-2) emphasizes the equipment interface boundaries; the simplified functional block diagram (Figure 2-3) shows the major sub-system functional relationships; and the equivalent functional block diagram (Figure 2-4) presents a detailed (although not completely accurate) model of the tracking system AUTO mode. Section 3.0 extracts from these figures a simplified equivalent functional block diagram of the Electronics Assembly and develops a set of equations defining the Electronics Assembly input/output transfer functions.

3.1 SMALL SIGNAL ELECTRONICS ASSEMBLY DIAGRAM

Figure 3-1 shows a simplified equivalent functional block diagram for the CSM HGA small signal Electronics Assembly. It is a simplified combination of Figures 2-3 and 2-4 which assumes

1. Small signal, linear approximations
2. Earth Presence
3. No excessive tracking error (less than $\pm 1°$)
4. No scan limit effects
5. No whiparound

These assumptions remove non-linear effects and all logic switching except the A-C/B-C tracking mode selection. The use of this linear model is valid only for small tracking errors, up to about ± 0.1 degrees or less.

The inputs to this model are the Transponder (receiver) output V_R (Interface B of Figure 2-2), the A, B, and C Axis Tachometer outputs V_{T1}, V_{T2}, and V_{T3} (Interface C), and the B and C Axis Induction Potentiometer (BIP and CIP) outputs V_β and V_γ (Interface C). The outputs from this model are the A, B, and C Axis servo motor drive voltages V_{P1}, V_{P2}, and V_{P3} (Interface C).

The receiver output V_R is processed by the demodulator K_D, which separates the azimuth and elevation signals into separate channels. K_D is made a function of j, the parameter value index. The correlation of j to the parameter values in Table 2-1 is

Assume: Earth Presence, no excessive Tracking Error, no Scan Limit effects, and no Whiparound

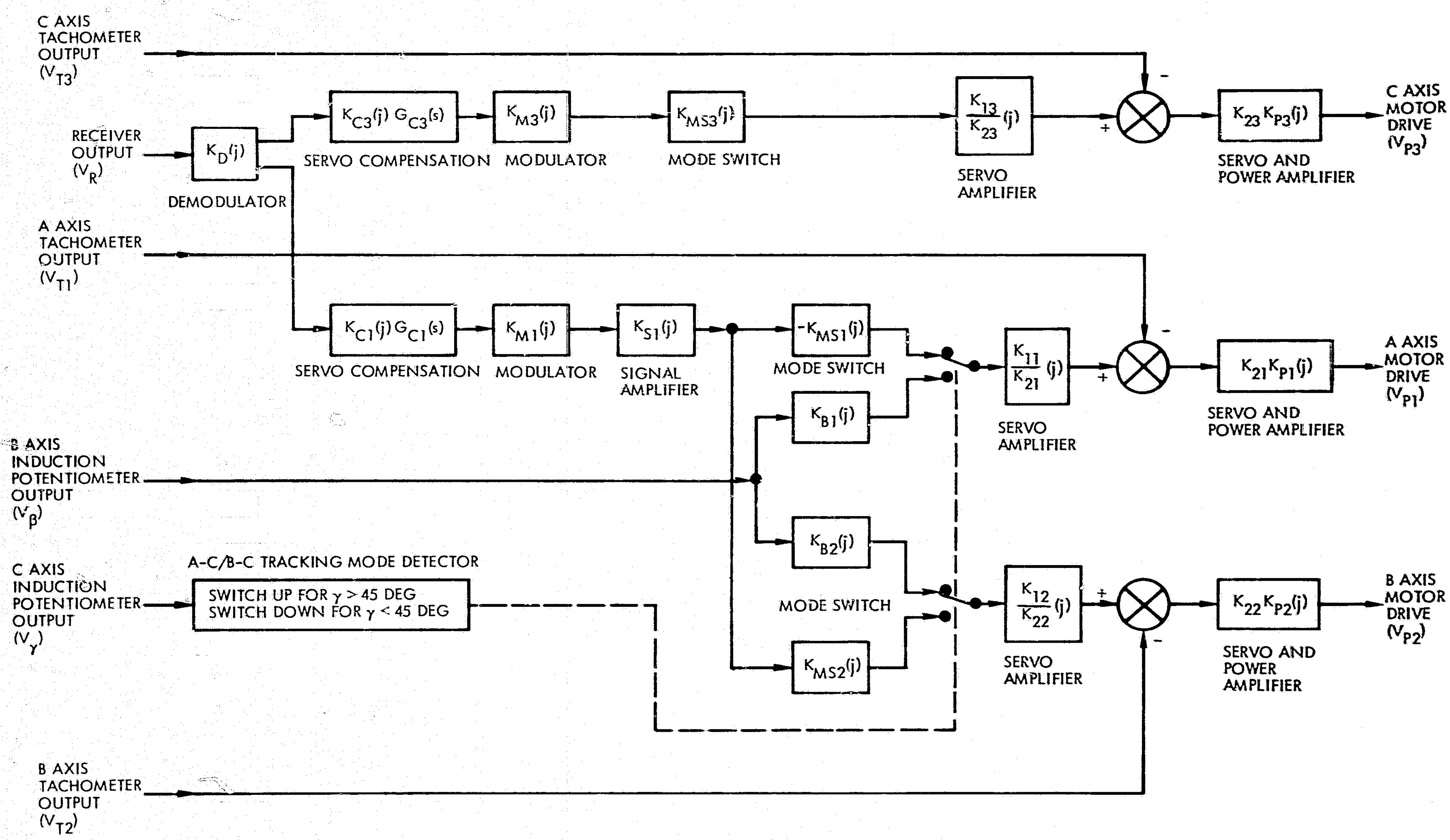

Small Signal Electronics Assembly
Simplified Equivalent Functional Block Diagram

Figure 3-1

$j = 1 \Rightarrow$ 77°F HI,
$j = 2 \Rightarrow$ 77°F NOM,
$j = 3 \Rightarrow$ 77°F LO,
$j = 4 \Rightarrow$ 200°F HI,
$j = 5 \Rightarrow$ 200°F NOM,
and $j = 6 \Rightarrow$ 200°F LO.

The elevation signal is processed by a servo compensation network $K_{C3}G_{C3}(s)$, a modulator K_{M3}, a mode switch K_{MS3}, and a servo and power amplifier combination K_{13}/K_{23} and $K_{23}K_{P3}$. The azimuth signal is processed by a servo compensation network $K_{C1}G_{C1}(s)$, a modulator K_{M1}, a signal amplifier K_{S1}, and, depending on whether γ is greater or less than 45°, by either mode switch K_{MS1} or K_{MS2} and either servo and power amplifier combination K_{11}/K_{21} and $K_{21}K_{P1}$ or K_{12}/K_{22} and $K_{22}K_{P2}$. The BIP signal V_β is processed by either mode switch K_{B2} or K_{B1} and either servo and power amplifier combination K_{12}/K_{22} and $K_{22}K_{P2}$ or K_{11}/K_{21} and $K_{21}K_{P1}$. The A, B, and C Axis Tachometer outputs V_{T1}, V_{T2}, and V_{T3} are processed by the servo and power amplifier combinations as shown.

The C Axis Induction Pot (CIP) signal is used in this model only to determine the tracking mode. The "A-C" tracking mode exists when $\gamma > 45°$, and the "B-C" tracking mode exists when $\gamma < 45°$:

1. A-C Tracking Mode ($\gamma > 45°$)
   a. Azimuth tracking is performed by the A Axis.
   b. Elevation tracking is performed by the C Axis.
   c. The B Axis is closed upon itself, the B Axis Induction Pot (BIP) signal controlling the B Axis Motor Drive V_{P2} as an error signal. This connection keeps the B Axis Gimbal angle β near zero.
2. B-C Tracking Mode ($\gamma < 45°$)
   a. Azimuth tracking is performed by the B Axis.
   b. Elevation tracking is performed by the C Axis.
   c. The A Axis is closed through the B Axis, the BIP signal

controlling the A Axis Motor Drive V_{P1} as an error signal. This connection also keeps the B Axis Gimbal angle β near zero; non-zero β values produce changes in the A Axis Gimbal angle α that tend to cause β to be driven to zero.

3.2 SMALL SIGNAL ELECTRONICS ASSEMBLY TRANSFER FUNCTIONS

Transfer functions for the small signal Electronics Assembly can be determined by multiplying together the various gains in Figure 3-1. For the A-C Tracking Mode, the Figure 3-1 switch is in the "UP" position, yielding the "A-C Tracking Mode" formulas in Figure 3-2. Note that the sign of K_{MS1} is negative, so that the V_R coefficient for $V_{P1\ (A-C)}$ is negative. This negative signal is required to cancel the "-" effect of the - cos β sin γ term between ω_{1X} and ω_{3y} in Figure 2-4.

For the B-C Tracking Mode, the Figure 3-1 switch is in the "DOWN" position, yielding the "B-C Tracking Mode" formulas in Figure 3-2. The C Axis Motor Drive formulas are the same for both the A-C and B-C Tracking Modes.

To determine the limits of these transfer functions, the multiplications indicated can be performed for each of the six j index values. The limits will correspond to those resulting coefficients having maximum and minimum values.

A-C Tracking Mode:

A Axis Motor Drive
$$V_{P1(A-C)}(j) = K_{21}K_{P1}(j)\left\{\left[-K_D(j)K_{C1}(j)G_{C1}(s)K_{M1}(j)K_{S1}(j)K_{MS1}(j)\frac{K_{11}}{K_{21}}(j)\right]V_R - V_{T1}\right\}$$

B Axis Motor Drive
$$V_{P2(A-C)}(j) = K_{22}K_{P2}(j)\left\{\left[K_{B2}(j)\frac{K_{12}}{K_{22}}(j)\right]V_\beta - V_{T2}\right\}$$

C Axis Motor Drive
$$V_{P3(A-C)}(j) = K_{23}K_{P3}(j)\left\{\left[K_D(j)K_{C3}(j)G_{C3}(s)K_{M3}(j)K_{MS3}(j)\frac{K_{13}}{K_{23}}(j)\right]V_R - V_{T3}\right\}$$

B-C Tracking Mode:

A Axis Motor Drive
$$V_{P1(B-C)}(j) = K_{21}K_{P1}(j)\left\{\left[K_{B1}(j)\frac{K_{11}}{K_{21}}(j)\right]V_\beta - V_{T1}\right\}$$

B Axis Motor Drive
$$V_{P2(B-C)}(j) = K_{22}K_{P2}(j)\left\{\left[K_D(j)K_{C1}(j)G_{C1}(s)K_{M1}(j)K_{S1}(j)K_{MS2}(j)\frac{K_{12}}{K_{22}}(j)\right]V_R - V_{T2}\right\}$$

C Axis Motor Drive
$$V_{P3(B-C)}(j) = V_{P3(A-C)}(j)$$

Small Signal Electronics Assembly Transfer Function Formulas

Figure 3-2

4.0 SMALL SIGNAL TRANSFER FUNCTION COEFFICIENTS

The previous sections of this report have presented background material leading up to estimates of the nominal and worst-case limits of the small signal Electronics Assembly input/output transfer functions. Section 3.0 develops equations for these functions, which give the symbollic relationships between the A, B, and C Axis servo motor drive voltages and the receiver output, BIP output, and the A, B, and C Axis tachometer outputs. The CIP output is included in the model merely to define the A-C and B-C tracking modes. Section 4.0 presents tabulated and plotted results of parameter substitutions from Table 2-1 into the equations of Section 3.0.

4.1 DATA PRESENTATION FORMAT

The Section 3.0 transfer function equations, Figure 3-2, which state the relationships between the motor drive voltages and the receiver, BIP, and tachometer outputs, have three characteristics which, due to the linearity assumption, can be considered separately. First, the receiver-to-power-amplifier effects, the BIP-to-power-amplifier effects, and the tachometer-to-power-amplifier effects may be separated from each other. Any composite effects can be determined by adding the appropriate separate effects.

Second, the quasi-static (DC) effects may be separated from the frequency-dependent effects contributed by $G_C(s)$. The net effects at any frequency can be determined by multiplying the $\omega = 0$ receiver-to-power-amplifier transfer characteristics (for which $G_C(s) = 1$) by the appropriate scaling factors from the $G_C(s)$ (only) gain versus frequency plots.

Third, the useable motor drive voltages are not given directly by the V_{Pi} formulas in Figure 3-2. Specifically, the motors operate only on that portion of the drive signals that is in phase-quadrature (90° out-of-phase) with the 400 Hz reference. Thus, any phase shifts introduced in the system between the servo compensation networks and the motors will reduce the effective motor drives by a multiplicative factor equal to the Cosine of the net phase shifts. As mentioned in paragraph 2.2, phase shifts are introduced by the modulators (ϕ_{K_M}), the mode switches ($\phi_{K_{MS}}$, $\phi_{K_{B1}}$, and $\phi_{K_{B2}}$), the tachometers (ϕ_{K_T}), and the power amplifiers (ϕ_{K_P}).* The effect of the net phase shifts can be included in the model of Figure 3-1 by lumping these phase shifts in the mode switches and tachometers. That is, define

$$K'_{MS} = K_{MS} \cos (\phi_{K_M} + \phi_{K_{MS}} + \phi_{K_P}),$$

$$K'_{B1} = K_{B1} \cos (\phi_{K_{B1}} + \phi_{K_{P1}}),$$

$$K'_{B2} = K_{B2} \cos (\phi_{K_{B2}} + \phi_{K_{P2}}),$$

and

$$K'_{T} = K_{T} \cos (\phi_{K_T} + \phi_{K_P}).$$

On the basis of the foregoing discussion, the tabulated and plotted small signal Electronics Assembly transfer function results are separated into three groups. The first group presents detailed tabulations of the receiver-to-power-amplifier, BIP-to-power-amplifier, and tachometer-to-power-amplifier DC characteristics both with and without phase shift effects. The second group presents tabulations and plots of the frequency-dependent characteristics of the servo compensation $G_C(s)$ terms. And the third group gives condensed tabulations and plots for the worst-case extremes (envelopes) of the DC transfer functions.

4.2 PARAMETER SUBSTITUTION APPROACH

The substitution of parameter values from Table 2-1 into the equations of Figure 3-2 follows a modified absolute worst-case analysis criterion: At each of the two temperatures 77°F and 200°F, all of the parameters are simultaneously assigned either high, nominal, or low values. Such an approach sometimes places an unreasonable constraint on a system's design, since the condition where all parameters actually achieve simultaneous extreme values is rather unlikely; the system might be "worst-cased" out of being able to operate satisfactorily. On the other hand, a system that

* The modulators, induction potentiometers, and tachometers ideally represent "+" signals as 400 Hz signals with +90° shifts and "-" signals as 400 Hz signals with -90° shifts. ϕ_{K_M} and ϕ_{K_T} represent phase shifts from ±90°.

is able to provide satisfactory operation, even with absolute worst-case parameters, can be guaranteed to operate under actual conditions. Another way of looking at this approach is that it provides maximum limits within which the system must operate.

4.3 SMALL SIGNAL TABULATED RESULTS

A tabulation of the small signal Electronics Assembly transfer function quasi-static (DC) coefficients is given in Tables 4-1 and 4-2. Table 4-1 presents the function coefficients in the absence of phase shifts. These coefficients can be used to predict the magnitude of the power amplifier outputs for a given set of input levels. Since phase shift effects have been ignored, these coefficients are directly related to measurable signals. Table 4-2 gives the function coefficients, including phase shifts, and, as such, represents the effective Electronics Assembly contribution to the overall system performance.

The tabulations in Tables 4-1 and 4-2 reference the receiver-to-power-amplifier gain terms of the Figure 3-2 equations by the factor K_{RP} and the BIP-to-power-amplifier gains by K_{BP}. The Figure 3-2 equations can thus be reduced to the equivalent forms

$$V_{P1(A-C)} = -K_{RP1}(j)V_R - K_{21}K_{P1}(j)V_{T1},$$

$$V_{P2(A-C)} = K_{BP2}(j)V_\beta - K_{22}K_{P2}(j)V_{T2},$$

$$V_{P3(A-C)} = K_{RP3}(j)V_R - K_{23}K_{P3}(j)V_{T3},$$

$$V_{P1(B-C)} = K_{BP1}(j)V_\beta - K_{21}K_{P1}(j)V_{T1},$$

$$V_{P2(B-C)} = K_{RP2}(j)V_R - K_{22}K_{P2}(j)V_{T2},$$

and

$$V_{P3(B-C)} = V_{P3(A-C)},$$

where K_{RP1} is the A Axis gain between V_R and V_{P1}, K_{RP2} is the B Axis gain between V_R and V_{P2}, K_{RP3} is the C Axis gain between V_R and V_{P3}, K_{BP1} is the A Axis gain between V_β and V_{P1}, and K_{BP2} is the B Axis gain between

Index j	Condition	$-K_{RP1}(j)$	$K_{RP2}(j)$	$K_{RP3}(j)$	$K_{BP1}(j)$	$K_{BP2}(j)$	$-K_{21}K_{P1}(j)$	$-K_{22}K_{P2}(j)$	$-K_{23}K_{P3}(j)$
1	77°F HI	-1011	1066	919	316	1210	-168	-86	-86
2	77°F NOM	- 702	697	653	244	846	-137	-70	-70
3	77°F LO	- 410	378	345	156	456	- 92	-47	-47
4	200°F HI	-1000	984	764	308	1314	-164	-84	-84
5	200°F NOM	- 672	634	553	234	900	-131	-67	-67
6	200°F LO	- 398	346	333	155	392	- 91.5	-46.7	-46.7

$$-K_{RP1}(j) = -K_D(j)K_{C1}(j)K_{M1}(j)K_{S1}(j)K_{MS1}(j)\frac{K_{11}}{K_{21}}(j)K_{21}K_{P1}(j)$$

$$K_{RP2}(j) = K_D(j)K_{C1}(j)K_{M1}(j)K_{S1}(j)K_{MS2}(j)\frac{K_{12}}{K_{22}}(j)K_{22}K_{P2}(j)$$

$$K_{RP3}(j) = K_D(j)K_{C3}(j)K_{M3}(j)K_{MS3}(j)\frac{K_{13}}{K_{23}}(j)K_{23}K_{P3}(j)$$

$$K_{BP1}(j) = K_{B1}(j)\frac{K_{11}}{K_{21}}(j)K_{21}K_{P1}(j)$$

$$K_{BP2}(j) = K_{B2}(j)\frac{K_{12}}{K_{22}}(j)K_{22}K_{P2}(j)$$

Note: Small Amplitude DC Signals Are Assumed; $G_C(s) = 1$.

Small Amplitude DC Coefficients (without Phase Shifts)

Table 4-1

Index j	Condition	$-K'_{RP1}(j)$	$-K'_{RP2}(j)$	$K'_{RP3}(j)$	$K'_{BP1}(j)$	$K'_{BP2}(j)$	$-K_{21}K'_{P1}(j)$	$-K_{22}K'_{P2}(j)$	$-K_{23}K'_{P3}(j)$
1	77°F HI	-479	536	798	308	1199	-163	-83.6	-83.6
2	77°F NOM	-498	506	499	240	842	-132	-67.6	-67.6
3	77°F LO	-342	321	201	155	432	- 89.1	-45.5	-45.5
4	200°F HI	-131	257	323	257	1014	-127	-64.8	-64.8
5	200°F NOM	-249	201	201	193	741	- 95.5	-48.8	-48.8
6	200°F LO	-211	181	147	132	385	- 65.9	-33.6	-33.6

$$-K'_{RP1}(j) = -K_D(j)K_{C1}(j)K_{M1}(j)K_{S1}(j)K_{MS1}(j)\frac{K_{11}}{K_{21}}(j)K_{21}K_{P1}(j)\text{Cos}[\phi_{K_{M1}}(j) + \phi_{K_{MS1}}(j) + \phi_{K_{P1}}(j)]$$

$$K'_{RP2}(j) = K_D(j)K_{C1}(j)K_{M1}(j)K_{S1}(j)K_{MS2}(j)\frac{K_{12}}{K_{22}}(j)K_{22}K_{P2}(j)\text{Cos}[\phi_{K_{M1}}(j) + \phi_{K_{MS2}}(j) + \phi_{K_{P2}}(j)]$$

$$K'_{RP3}(j) = K_D(j)K_{C3}(j)K_{M3}(j)K_{MS3}(j)\frac{K_{13}}{K_{23}}(j)K_{23}K_{P3}(j)\text{Cos}[\phi_{K_{M3}}(j) + \phi_{K_{MS3}}(j) + \phi_{K_{P3}}(j)]$$

$$K'_{BP1}(j) = K_{B1}(j)\frac{K_{11}}{K_{21}}(j)K_{21}K_{P1}(j)\text{Cos}[\phi_{K_{B1}}(j) + \phi_{K_{P1}}(j)]$$

$$K'_{BP2}(j) = K_{B2}(j)\frac{K_{12}}{K_{22}}(j)K_{22}K_{P2}(j)\text{Cos}[\phi_{K_{B2}}(j) + \phi_{K_{P2}}(j)]$$

$$-K_{21}K'_{P1}(j) = -K_{21}K_{P1}(j)\text{Cos}[\phi_{K_{P1}}(j)]$$

$$-K_{22}K'_{P2}(j) = -K_{22}K_{P2}(j)\text{Cos}[\phi_{K_{P2}}(j)]$$

$$-K_{23}K'_{P3}(j) = -K_{23}K_{P3}(j)\text{Cos}[\phi_{K_{P3}}(j)]$$

Small Amplitude DC Coefficients (with Phase Shifts)

Table 4-2

V_β and V_{P2}. The formulas for these factors (as used) are given in Tables 4-1 and 4-2, respectively. Note that the effects of phase shifts within the tachometers themselves have not been included in the K_2K_P' formulations, so the net effect of the tachometers on the motors is not completely represented here.*

The interesting characteristics of Tables 4-1 and 4-2 are the coefficient variations. The coefficient variations from nominal at 77°F and 200°F, as well as the variations between 77°F and 200°F, are documented in Table 4-3. For example, the K_{RP1} factor varies about +44% (+3.2 db) and -42% (-4.7 db) from nominal at 77°F and about +49% (+3.4 db) and -41% (-4.6 db) from nominal at 200°F. The K_{RP1} high value varies about -1% (-0.1 db) going from 77°F to 200°F, while the nominal and low values vary about -4% (-0.4 db) and -3% (-0.3 db), respectively.

Table 4-4 documents the variations between the coefficients without phase shift effects (Table 4-1) and those with phase shifts (Table 4-2). For example, the 77°F HI K_{RP1}' value is 53% (6.5 db) below the corresponding K_{RP1} value, indicating a 53% (6.5 db) effective signal loss due to phase shifts. The largest loss, -87% (-17.7 db), is experienced by K_{RP1}' at 200°F HI.

4.4 SMALL SIGNAL SERVO COMPENSATION $G_C(s)$ FREQUENCY CHARACTERISTICS

The small signal Servo Compensation terms $G_{C1}(s)$ and $G_{C3}(s)$ are approximated in this report by

A/B Axis Compensation $$G_{C1}(s) = \frac{(0.234s + 1)}{(0.015s + 1)(1.22s + 1)} = \frac{\left(\frac{s}{4.275} + 1\right)}{\left(\frac{s}{0.82} + 1\right)\left(\frac{s}{66.67} + 1\right)}$$

C Axis Compensation $$G_{C3}(s) = \frac{(0.166s + 1)}{(0.0125s + 1)(0.883s + 1)} = \frac{\left(\frac{s}{6} + 1\right)}{\left(\frac{s}{1.2} + 1\right)\left(\frac{s}{80} + 1\right)}$$

The frequency characteristics of these $G_C(s)$ terms are presented five ways for maximum utility.

* The net tachometer effects are given by $\omega_M K_T K_2 K_P \mathrm{Cos}(\phi_{K_T} + \phi_{K_P})$; only $K_2 K_P \mathrm{Cos}\phi_{K_P}$ is given in Table 4-2.

Approximate Variations	K_{RP1}		K_{RP2}		K_{RP3}		K_{BP1}		K_{BP2}		$K_{21}K_{P1}$		$K_{22}K_{P2}$		$K_{23}K_{P3}$	
	%	db	%	db	%	db	%	db	%	db	%	db	%	db	%	db
77°F NOM→HI	+44	+3.2	+53	+3.7	+41	+3.0	+30	+2.2	+43	+3.1	+23	+1.8	+23	+1.8	+23	+1.8
77°F NOM→LO	-42	-4.7	-46	-5.3	-47	-5.5	-36	-3.9	-46	-5.4	-33	-3.5	-33	-3.5	-33	-3.5
200°F NOM→HI	+49	+3.5	+55	+3.8	+38	+2.8	+32	+2.4	+46	+3.3	+25	+1.9	+25	+2.0	+25	+2.0
200°F NOM→LO	-41	-4.6	-45	-5.3	-40	-4.4	-34	-3.6	-57	-7.2	-30	-3.1	-30	-3.1	-30	-3.1
77°→200°F HI	- 1	-0.1	- 8	-0.7	-17	-1.6	- 3	-0.2	+ 9	+0.7	- 2	-0.2	- 2	-0.2	- 2	-0.2
77°→200°F NOM	- 4	-0.4	- 9	-0.8	-15	-1.4	- 4	-0.4	+ 6	+0.5	- 4	-0.4	- 4	-0.4	- 4	-0.4
77°→200°F LO	- 3	-0.3	- 8	-0.8	- 3	-0.3	- 1	-0.1	-14	-1.3	- 1	-0.1	- 1	-0.1	- 1	-0.1

Approximate Variations	K'_{RP1}		K'_{RP2}		K'_{RP3}		K'_{BP1}		K'_{BP2}		$K_{21}K'_{P1}$		$K_{22}K'_{P2}$		$K_{23}K'_{P3}$	
	%	db	%	db	%	db	%	db	%	db	%	db	%	db	%	db
77°F NOM→HI	- 4	- 0.3	+ 6	+0.5	+60	+4.1	+28	+2.2	+42	+3.1	+23	+1.8	+24	+1.9	+24	+1.9
77°F NOM→LO	-31	- 3.3	-37	-3.9	-60	-7.9	-35	-3.8	-49	-5.8	-33	-3.4	-33	-3.4	-33	-3.4
200°F NOM→HI	-47	- 5.6	+23	+2.1	+61	+4.1	+33	+2.5	+37	+2.7	+33	+2.5	+33	+2.5	+33	+2.5
200°F NOM→LO	-15	- 1.4	-10	-0.9	-28	-2.7	-32	-3.3	-48	-5.7	-31	-3.2	-31	-3.2	-31	-3.2
77°→200°F HI	-73	-11.3	-52	-6.4	-60	-7.9	-17	-1.6	-15	-1.4	-22	-2.2	-23	-2.2	-23	-2.2
77°→200°F NOM	-50	- 6.0	-60	-8.0	-60	-7.9	-20	-1.9	-12	-1.1	-28	-2.8	-28	-2.8	-28	-2.8
77°→200°F LO	-38	- 4.2	-44	-5.0	-27	-2.7	-15	-1.4	-11	-1.0	-26	-2.6	-26	-2.6	-26	-2.6

Approximate DC Coefficient Variations

Table 4-3

Approximate Variations	$K_{RP1} \to K'_{RP1}$		$K_{RP2} \to K'_{RP2}$		$K_{RP3} \to K'_{RP3}$		$K_{BP1} \to K'_{BP1}$		$K_{BP2} \to K'_{BP2}$		$K_{21}K_{P1} \to K_{21}K'_{P1}$		$K_{22}K_{P2} \to K_{22}K'_{P2}$		$K_{23}K_{P3} \to K_{23}\tilde{K}'_{P3}$	
	%	db	%	db	%	db	%	db	%	db	%	db	%	db	%	db
77°F HI	-53	- 6.5	-50	- 6.0	-13	-1.2	- 3	-0.2	- 1	-0.1	- 3	-0.3	- 3	-0.3	- 3	-0.3
77°F NOM	-29	- 3.0	-27	- 2.8	-24	-2.3	- 2	-0.1	- 0	-0.1	- 4	-0.3	- 3	-0.3	- 3	-0.3
77°F LO	-17	- 1.6	-15	- 1.4	-42	-4.7	- 1	-0.1	- 5	-0.5	- 3	-0.3	- 3	-0.3	- 3	-0.3
200°F HI	-87	-17.7	-74	-11.7	-58	-7.5	-17	-1.6	-23	-2.2	-23	-2.2	-23	-2.3	-23	-2.3
200°F NOM	-63	- 8.6	-68	-10.0	-64	-8.8	-18	-1.7	-18	-1.7	-27	-2.7	-27	-2.8	-27	-2.8
200°F LO	-47	- 5.5	-48	- 5.6	-56	-7.1	-15	-1.4	- 2	-0.2	-28	-2.9	-28	-2.9	-28	-2.9

Approximate Coefficient Variations Due to Phase Shifts

Table 4-4

Table 4-5 tabulates the Gain (ratio and 20 $\log_{10}$) and Phase values for selected frequencies in Rad/Sec and Hz. Included for comparison purposes are the averages of values given in a similar table in Reference (2); these values, listed under the "Autonetics Average" columns, are the average of the 77°F NOM, 200°F MIN, and 200°F MAX values given by Autonetics in Table 4-2, p. 4-14 of Reference (2). A comparison of these values with the $G_C(s)$ values indicates that the $G_{C1}(s)$ and $G_{C3}(s)$ approximations used for this report are quite good up to about 1.0 Hz, where the approximations begin to diverge from the Autonetics data. As noted on p. 4-15, Reference (2),

> "Since the process that produces this [Servo Compensation] effect is non linear, the frequency responses shown in Table [4-2, Reference (2)] were determined using [a non-linear] computer circuit simulation. A response at 10 Hz was obtained and an equivalent first order filter fit to the response. Then the composite response was evaluated over the range of frequencies indicated."

In addition to the tabulations in Table 4-5, the $G_{C1}(s)$ and $G_{C3}(s)$ frequency characteristics are plotted in Figures 4-1 through 4-8. Figures 4-1 and 4-5 are standard Bode Plots of the $G_{C1}(s)$ and $G_{C3}(s)$ Gains (db) and Phases (Deg) versus ω (Rad/Sec), and Figures 4-2 and 4-6 are standard Bode Plots of the $G_{C1}(s)$ and $G_{C3}(s)$ Gains (db) and Phases (Deg) versus f (Hz). Figures 4-3 and 4-7 plot the $G_{C1}(s)$ and $G_{C3}(s)$ Gains (linear ratio) versus ω (Rad/Sec), while Figures 4-4 and 4-8 plot the $G_{C1}(s)$ and $G_{C3}(s)$ Gains (linear ratio) versus f (Hz).

While such a data presentation may appear somewhat redundant, it is intended to provide information directly without conversion for the convenience of the reader. The gains are expressed in both linear (ratio) and 20 $\log_{10}$ (db) form, and the frequencies are expressed in both Rad/Sec and Hertz.

Axis		A/B					C				
Function		$G_{C1}(s)$			Autonetics Average		$G_{C3}(s)$			Autonetics Average	
Frequency		Gain		Phase	Gain	Phase	Gain		Phase	Gain	Phase
Rad/Sec	Hz	Ratio	db	Deg	Ratio	Deg	Ratio	db	Deg	Ratio	Deg
(0.006)	0.001	(1.000)	(0)	- 0.4			(1.000)	(0)	- 0.2		
0.010	(0.002)	(1.000)	(0)	- 0.6			(1.000)	(0)	- 0.4		
(0.031)	0.005	0.999	(0)	- 1.8			(1.000)	(0)	- 1.2		
0.050	(0.008)	0.998	(0)	- 2.9			0.999	(0)	- 1.9		
(0.063)	0.010	0.997	(0)	- 3.6	0.997	- 3.6	0.999	(0)	- 2.4	0.998	- 2.8
0.100	(0.016)	0.993	- 0.6	- 5.7			0.997	(0)	- 3.9		
(0.314)	0.050	0.936	- 0.6	-17.0			0.967	- 0.3	-11.9		
0.500	(0.080)	0.860	- 1.3	-25.1			0.926	- 0.7	-18.2		
(0.628)	0.100	0.802	- 1.9	-29.6	0.803	-29.8	0.891	- 1.0	-22.1	0.889	-22.7
1.000	(0.159)	0.651	- 3.7	-38.3			0.777	- 2.2	-31.1		
2.000	(0.318)	0.419	- 7.6	-44.4			0.542	- 5.3	-42.0		
2.200	0.350	-----	-----	-----	0.395	-44.7	-----	-----	-----	0.508	-44.9
2.500	(0.398)	0.361	- 8.9	-43.7			0.469	- 6.6	-43.5		
(3.142)	0.500	0.313	-10.1	-41.8			0.402	- 7.9	-43.4		
5.000	(0.796)	0.248	-12.1	-35.5			0.303	-10.4	-40.3		
(6.283)	1.000	0.229	-12.8	-32.2	0.233	-35.0	0.271	-11.3	-37.4	0.266	-43.3
10.00	(1.592)	0.206	-13.7	-27.0			0.230	-12.8	-31.2		
(31.42)	5.000	0.175	-15.1	-31.5			0.189	-14.5	-30.1		
50.00	(7.958)	0.154	-16.3	-40.8			0.171	-15.4	-37.5		
(62.83)	10.00	0.140	-17.1	-46.4	0.104	-61.6	0.158	-16.0	-42.5	0.098	-65.6
100.0	(15.92)	0.107	-19.5	-58.3			0.125	-18.1	-54.1		
(314.2)	50.00	0.040	-28.0	-78.6			0.049	-26.1	-76.6		
500.0	(79.58)	0.025	-31.9	-82.8			0.032	-30.0	-81.5		
(628.3)	100.0	0.020	-33.9	-84.3			0.025	-32.0	-83.2		
1000.0	(159.2)	0.013	-37.9	-86.4			0.016	-35.9	-85.7		

Note: Numbers in () are approximate.

Servo Compensation Frequency Characteristics

Table 4-5

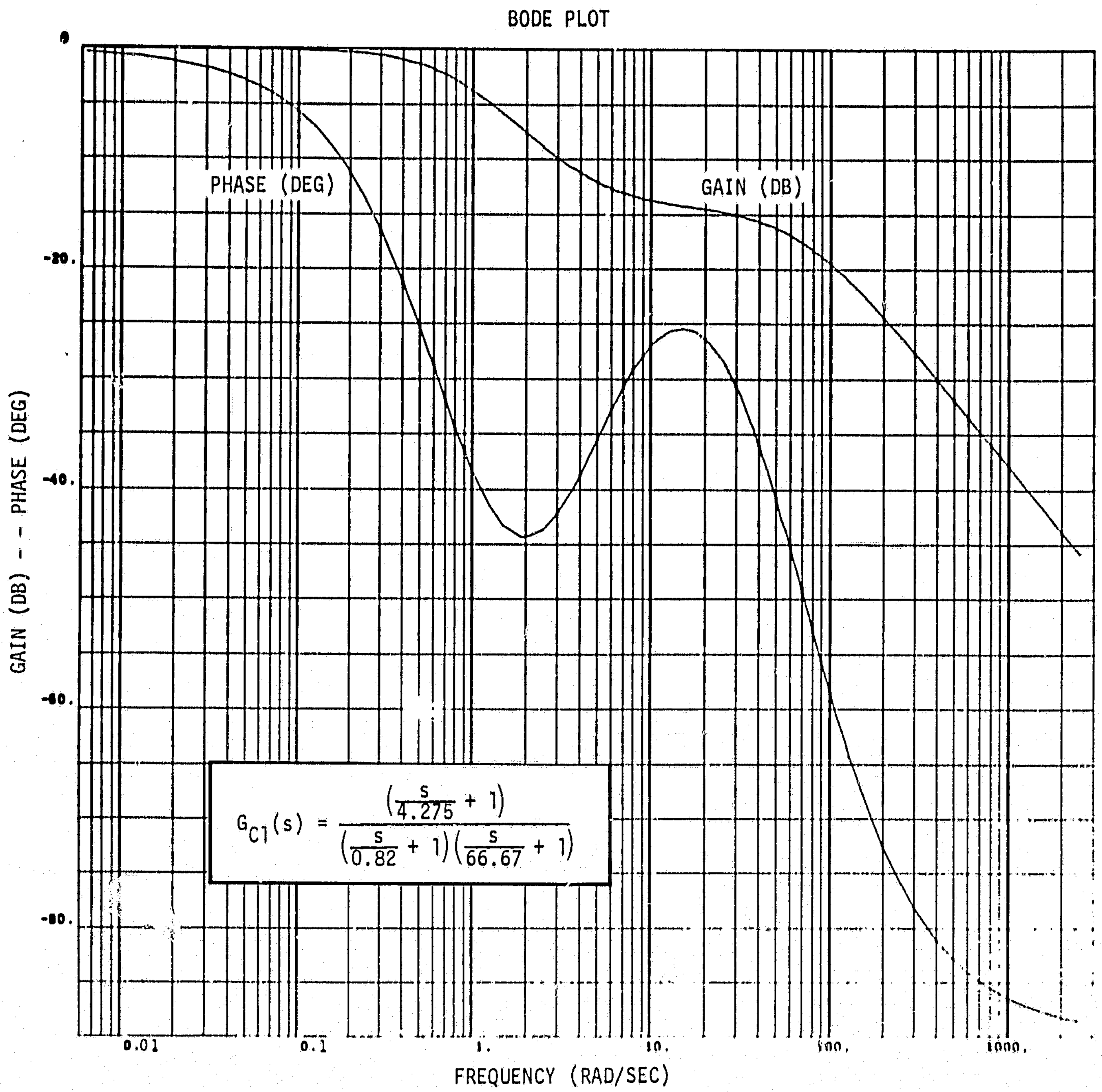

A/B Axis (Azimuth) Servo Compensation $G_{C1}(s)$
Gain (db) and Phase (Deg) Versus Frequency (Rad/Sec)

Figure 4-1

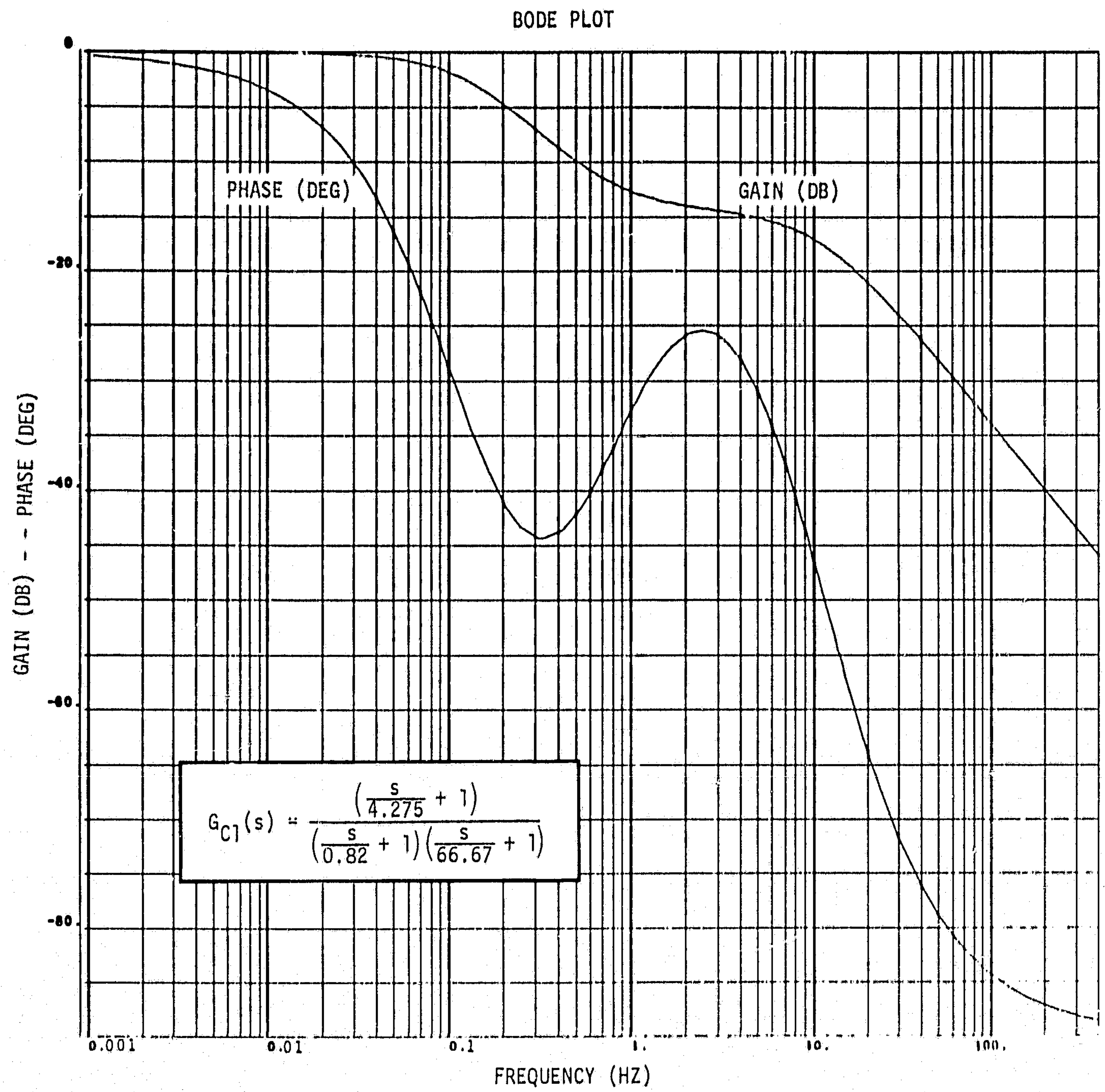

$$G_{C1}(s) = \frac{\left(\frac{s}{4.275} + 1\right)}{\left(\frac{s}{0.82} + 1\right)\left(\frac{s}{66.67} + 1\right)}$$

A/B Axis (Azimuth) Servo Compensation $G_{C1}(s)$
Gain (db) and Phase (Deg) Versus Frequency (Hz)

Figure 4-2

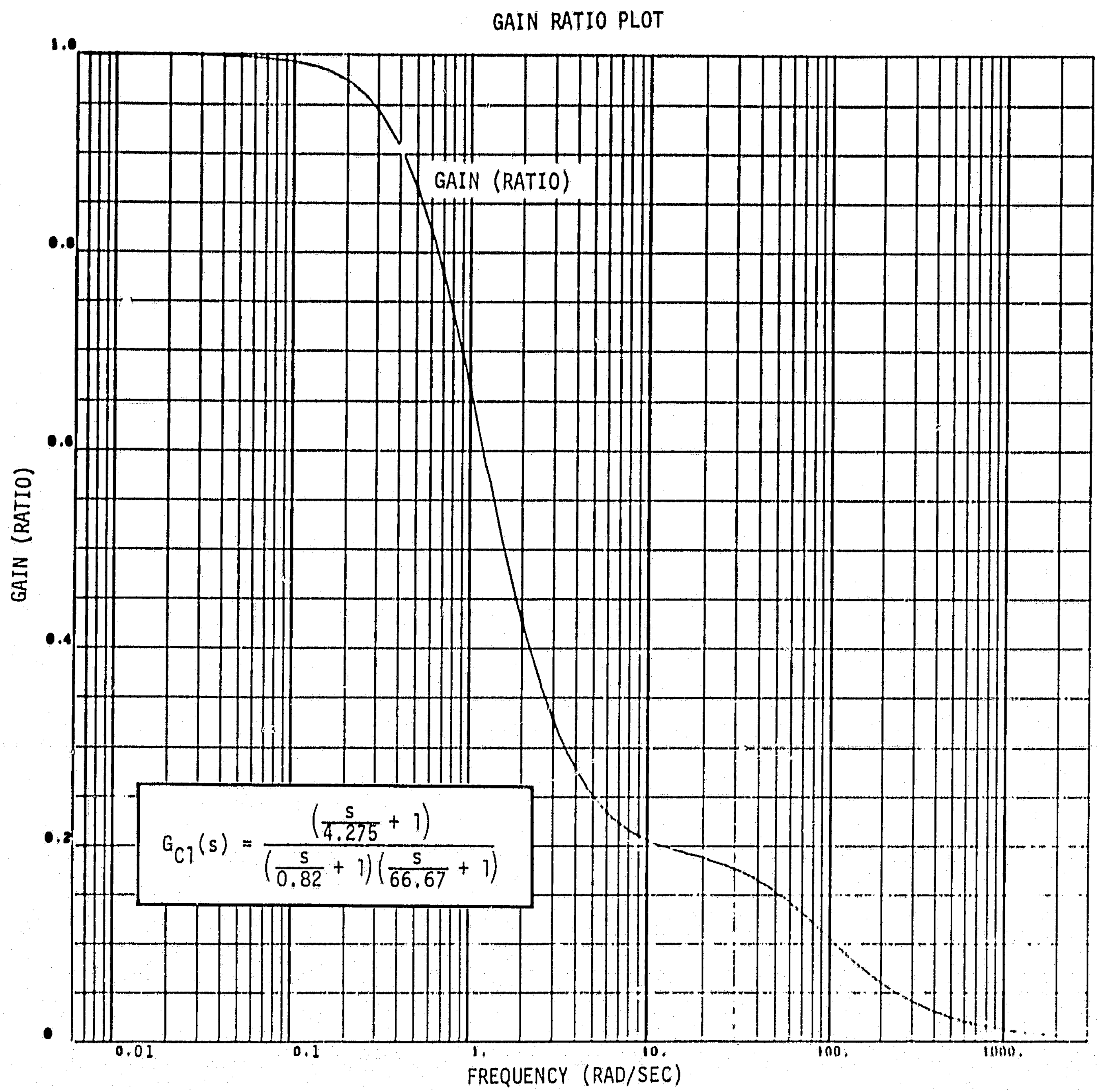

A/B Axis (Azimuth) Servo Compensation $G_{C1}(s)$
Gain (Ratio) Versus Frequency (Rad/Sec)

Figure 4-3

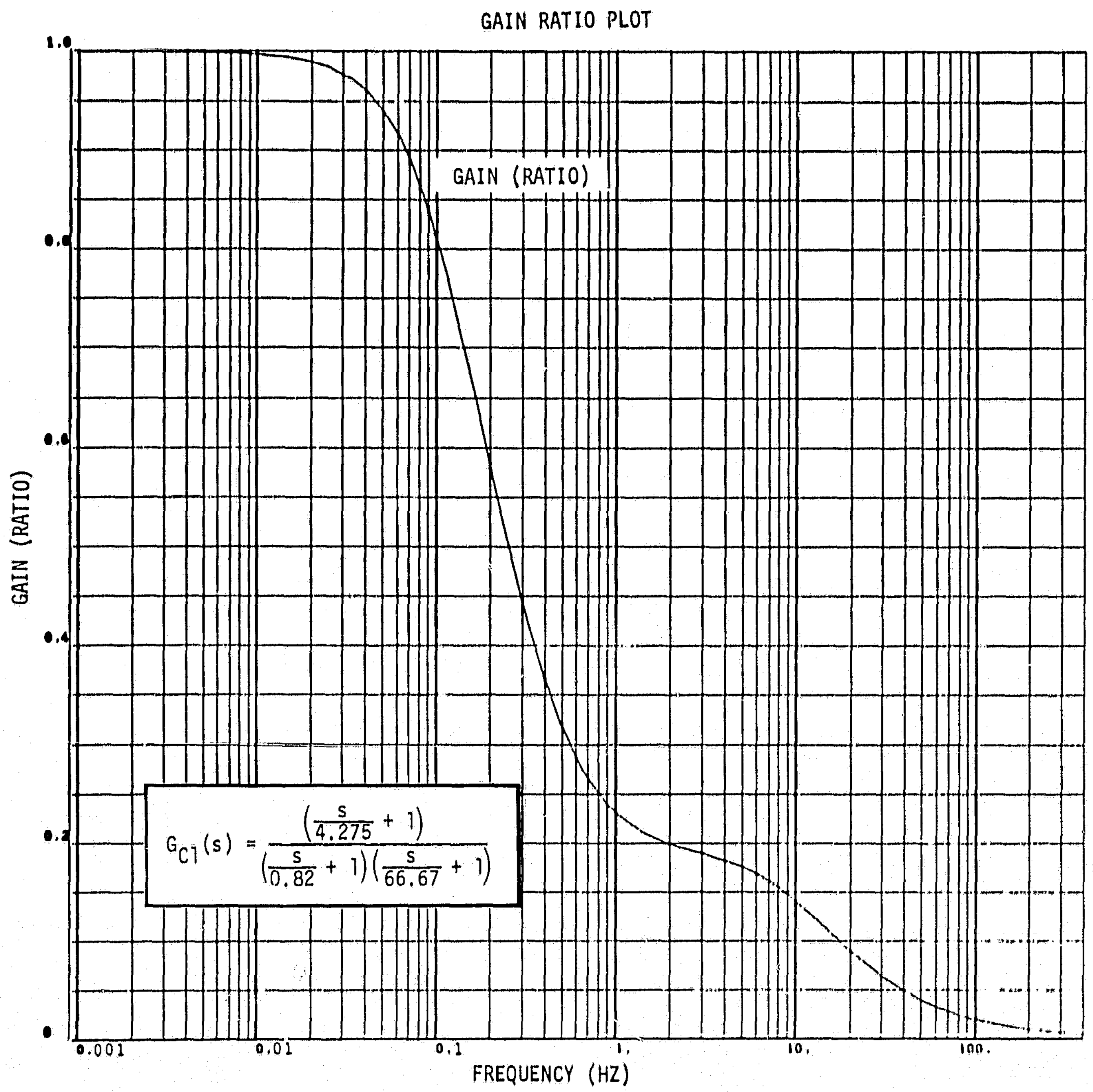

A/B Axis (Azimuth) Servo Compensation $G_{C1}(s)$
Gain (Ratio) Versus Frequency (Hz)

Figure 4-4

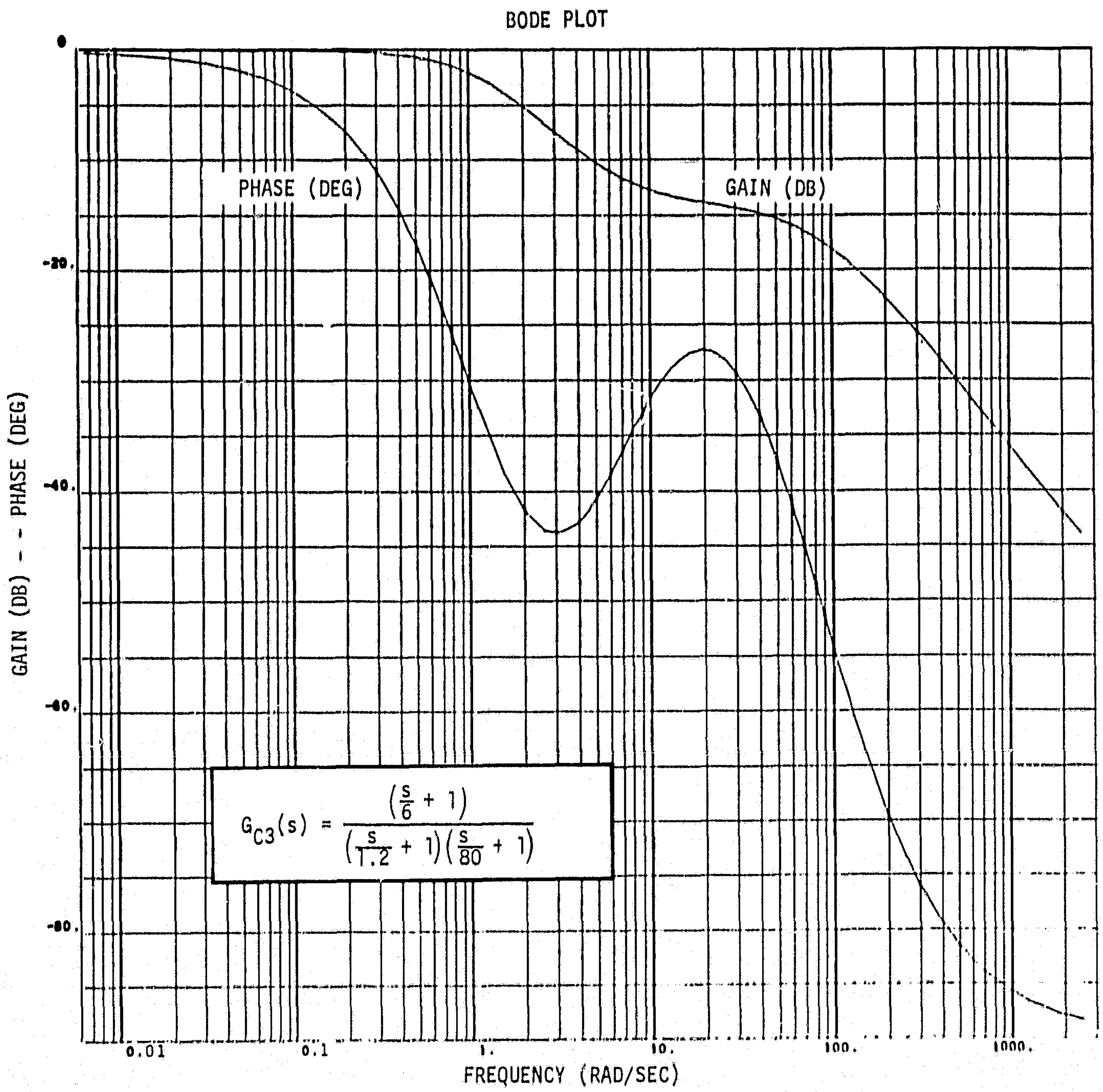

C Axis (Elevation) Servo Compensation $G_{C3}(s)$
Gain (db) and Phase (Deg) Versus Frequency (Rad/Sec)

Figure 4-5

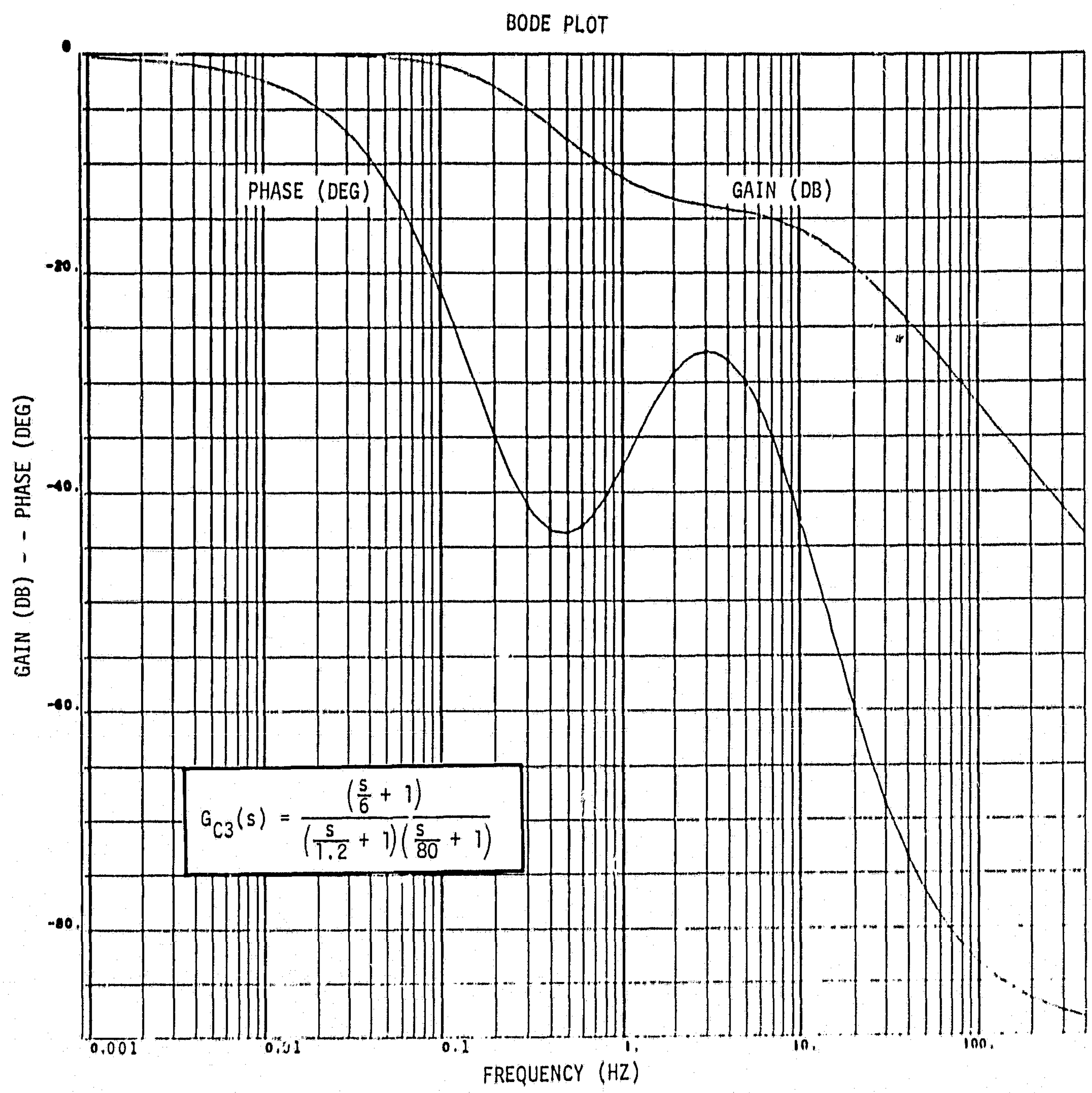

C Axis (Elevation) Servo Compensation $G_{C3}(s)$
Gain (db) and Phase (Deg) Versus Frequency (Hz)

Figure 4-6

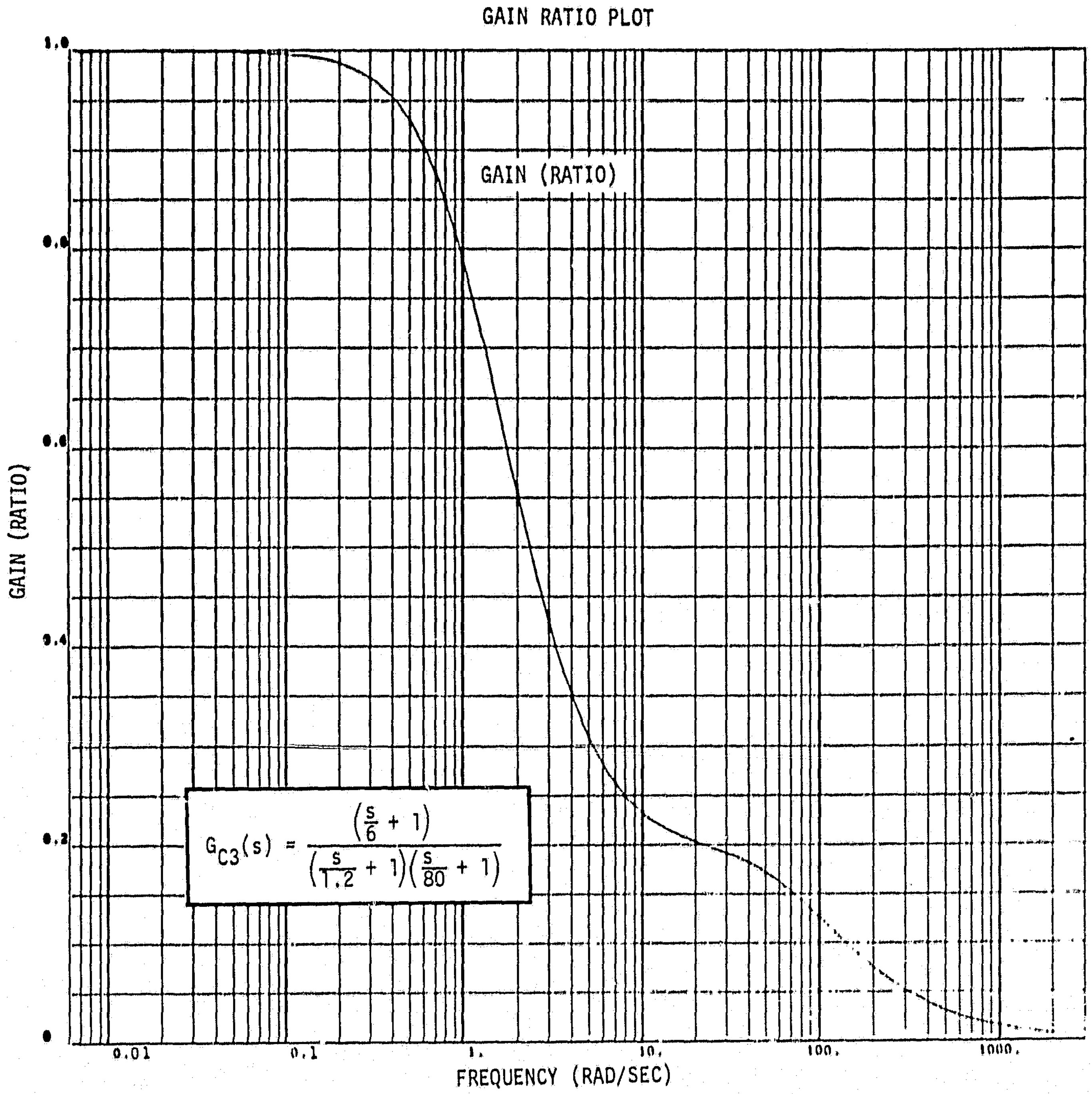

C Axis (Elevation) Servo Compensation $G_{C3}(s)$
Gain (Ratio) Versus Frequency (Rad/Sec)

Figure 4-7

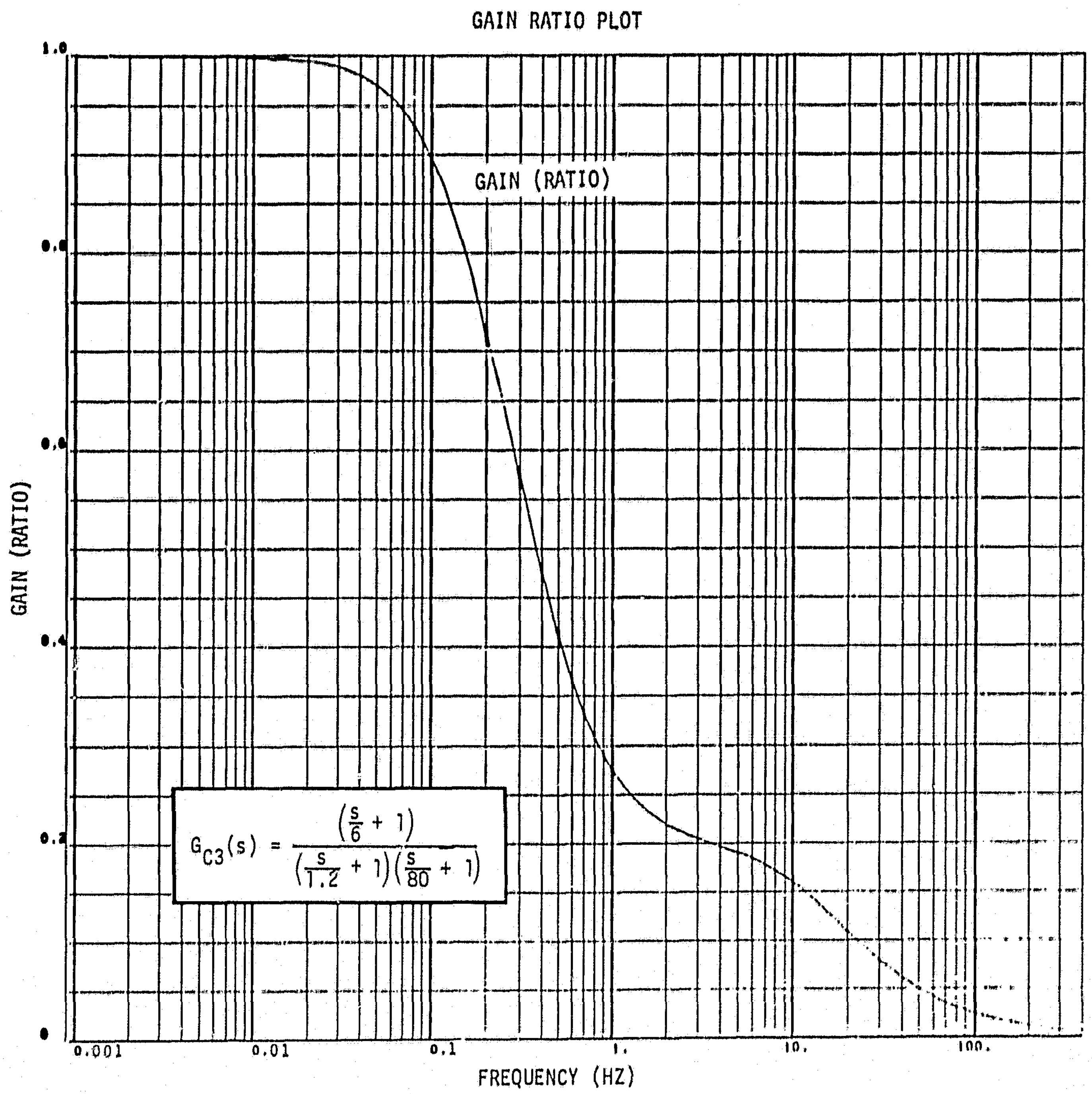

C Axis (Elevation) Servo Compensation $G_{C3}(s)$
Gain (Ratio) Versus Frequency (Hz)

Figure 4-8

4.5 SMALL SIGNAL TRANSFER FUNCTION LIMITS

Paragraph 4.3 documents the small signal Electronics Assembly transfer functions in terms of variations at 77°F and 200°F, and Paragraph 4.4 presents the small signal Servo Compensation frequency characteristics. The overall transfer function characteristics at a particular temperature and frequency can be determined by multiplying the appropriate gain factors. This approach can yield a large number of coefficient variation combinations.

However, the transfer function data can probably be better determined in terms of nominal and extreme values that apply to the entire operating temperature range. The procedure for determining the corresponding maximum, nominal, and mininum transfer function values would consist of calling-out the maximum and minimum values and averaging the 77°F and 200°F NOM values of Tables 4-1 and 4-2.

The data resulting from such a procedure is summarized in Table 4-6, which gives the maximum, nominal average, and minimum values taken from Tables 4-1 and 4-2. Analogous to Tables 4-3 and 4-4, Table 4-7 documents the limit variations between the nominal average and the maximum and minimum values for coefficients with and without included phase shift effects, as well as coefficient variations from those without to those with phase shifts. For example, K_{RP1} varies about +47% (+3.4 db) from nominal average to maximum and about -42% (-4.7 db) from nominal average to minimum. On the other hand, K'_{RP1} varies about +34% (+2.5 db) from nominal average to maximum and about -65% (-9.1 db) from nominal average to minimum. The K'_{RP1} maximum is about 51% (6.1 db) below the K_{RP1} maximum, while the K'_{RP1} nominal average and minimum values are down about -46% (-5.3 db) and -67% (-9.7 db), respectively.

The transfer function limit data presented in Table 4-6 can be further illustrated in the form of graphical plots. Figures 4-9 through 4-24 present the Small Signal Electronics Assembly DC transfer function limits in the following format: Variations with V_R, V_β, V_{T1}, V_{T2}, and V_{T3} are illustrated in separate graphs; separate graphs are given for variations with and without phase shift effects.

Condition	$-K_{RP1}$	K_{RP2}	K_{RP3}	K_{BP1}	K_{BP2}	$-K_{21}K_{P1}$	$-K_{22}K_{P2}$	$-K_{23}K_{P3}$
Maximum	-1011	1066	919	316	1314	-168	-86	-86
Nominal Average	- 687	666	603	239	873	-134	-68.5	-68.5
Minimum	- 398	346	333	155	392	- 91.5	-46.7	-46.7

Condition	$-K'_{RP1}$	K'_{RP2}	K'_{RP3}	K'_{BP1}	K'_{BP2}	$-K_{21}K'_{P1}$	$-K_{22}K'_{P2}$	$-K_{23}K'_{P3}$
Maximum	- 498	536	798	308	1199	-163	-83.6	-83.6
Nominal Average	- 373	353	350	216	791	-114	-58.2	-58.2
Minimum	- 131	181	147	132	385	- 65.9	-33.6	-33.6

Small Signal DC Transfer Function Limits

Table 4-6

Approximate Variation	K_{RP1}		K_{RP2}		K_{RP3}		K_{BP1}		K_{BP2}		$K_{21}K_{P1}$		$K_{22}K_{P2}$		$K_{23}K_{P3}$	
	%	db	%	db	%	db	%	db	%	db	%	db	%	db	%	db
Nom. Avg. → Max.	+47	+3.4	+60	+4.1	+ 52	+3.7	+32	+2.4	+50	+3.6	+25	+2.0	+26	+2.0	+26	+2.0
Nom. Avg. → Min.	-42	-4.7	-48	-5.7	- 45	-5.2	-35	-3.8	-55	-6.9	-32	-3.3	-32	-3.3	-32	-3.3

Approximate Variation	K'_{RP1}		K'_{RP2}		K'_{RP3}		K'_{BP1}		K'_{BP2}		$K_{21}K'_{P1}$		$K_{22}K'_{P2}$		$K_{23}K'_{P3}$	
	%	db	%	db	%	db	%	db	%	db	%	db	%	db	%	db
Nom. Avg. → Max.	+34	+2.5	+52	+3.6	+128	+7.2	+43	+3.1	+52	+3.6	+43	+3.1	+44	+3.1	+44	+3.1
Nom. Avg. → Min.	-65	-9.1	-49	-5.8	- 58	-7.5	-39	-4.3	-51	-6.3	-42	-4.8	-42	-4.8	-42	-4.8

Approximate Variation	$K_{RP1}\to K'_{RP1}$		$K_{RP2}\to K'_{RP2}$		$K_{RP3}\to K'_{RP3}$		$K_{BP1}\to K'_{BP1}$		$K_{BP2}\to K'_{BP2}$		$K_{21}K_{P1}\to K_{21}K'_{P1}$		$K_{22}K_{P2}\to K_{22}K'_{P2}$		$K_{23}K_{P3}\to K_{23}K'_{P3}$	
	%	db	%	db	%	db	%	db	%	db	%	db	%	db	%	db
Maximum	-51	-6.1	-50	-6.0	- 13	-1.2	- 3	-0.2	- 9	-0.8	- 3	-0.3	- 3	-0.3	- 3	-0.3
Nominal Average	-46	-5.3	-47	-5.5	- 42	-4.7	-10	-0.9	- 9	-0.8	-15	-1.4	-15	-1.4	-15	-1.4
Minimum	-67	-9.7	-48	-5.6	- 56	-7.1	-15	-1.4	- 2	-0.2	-28	-2.8	-28	-2.9	-28	-2.9

Approximate Small Signal DC Transfer Function Limit Variations

Table 4-7

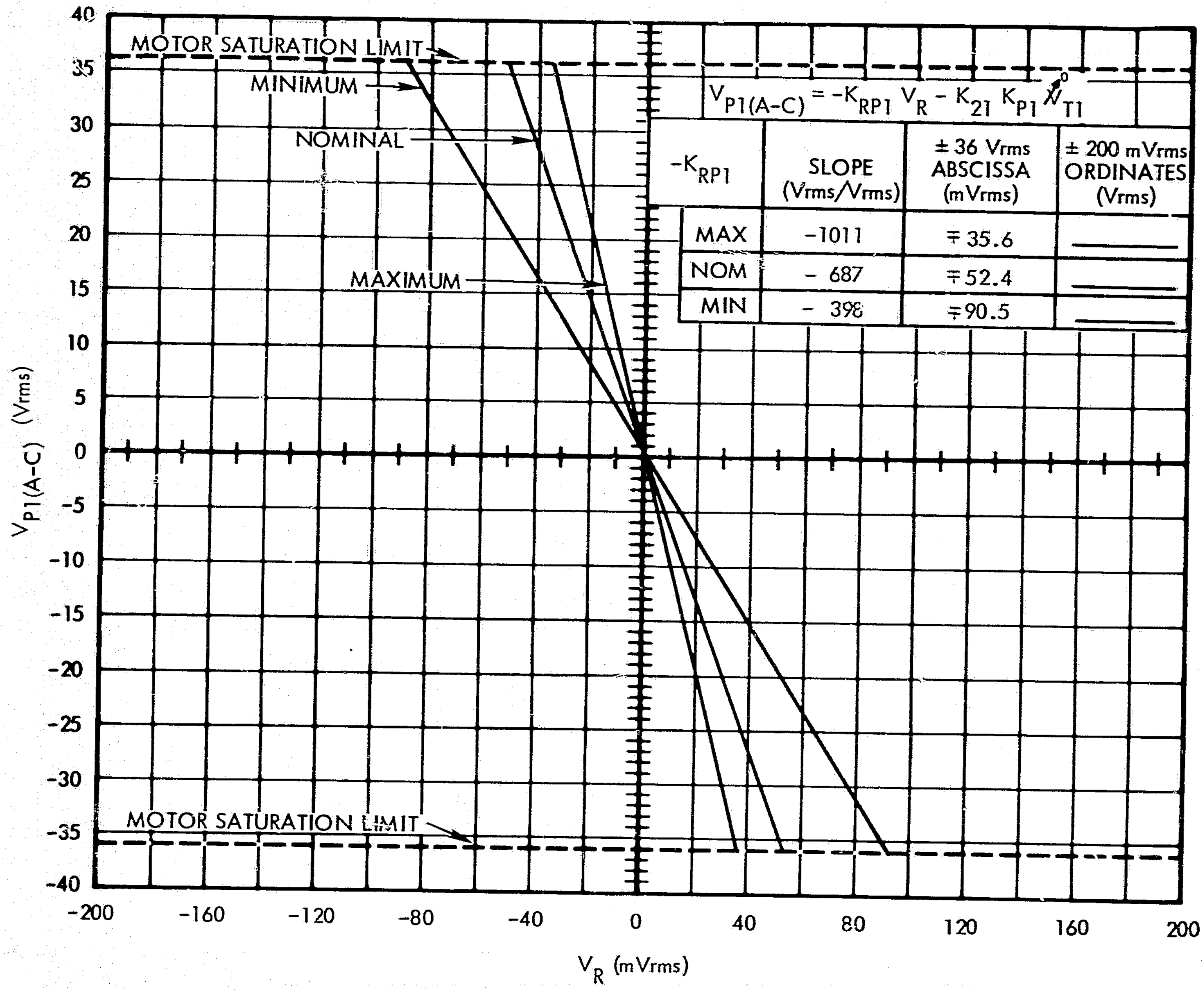

$-K_{RP1}$	SLOPE (Vrms/Vrms)	± 36 Vrms ABSCISSA (mVrms)	± 200 mVrms ORDINATES (Vrms)
MAX	-1011	∓ 35.6	______
NOM	- 687	∓ 52.4	______
MIN	- 398	∓ 90.5	______

A-C Tracking Mode; A Axis Motor Drive Limits
as a Function of Receiver Output
$V_{P1(A-C)}$ Versus V_R (Without Phase Shifts)

Figure 4-9

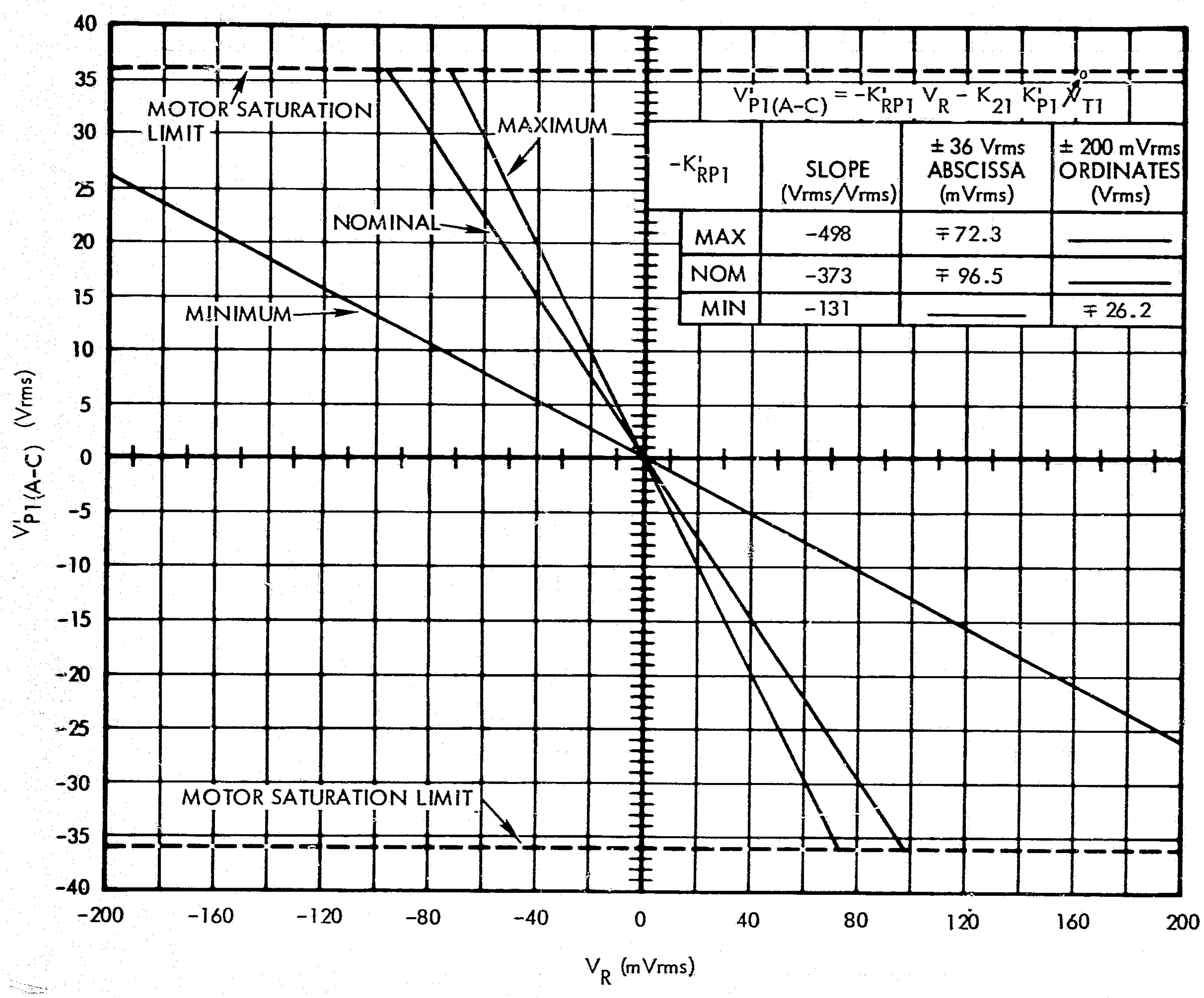

A-C Tracking Mode; A Axis Motor Drive Limits
as a Function of Receiver Output
$V'_{P1(A-C)}$ Versus V_R (With Phase Shifts)

Figure 4-10

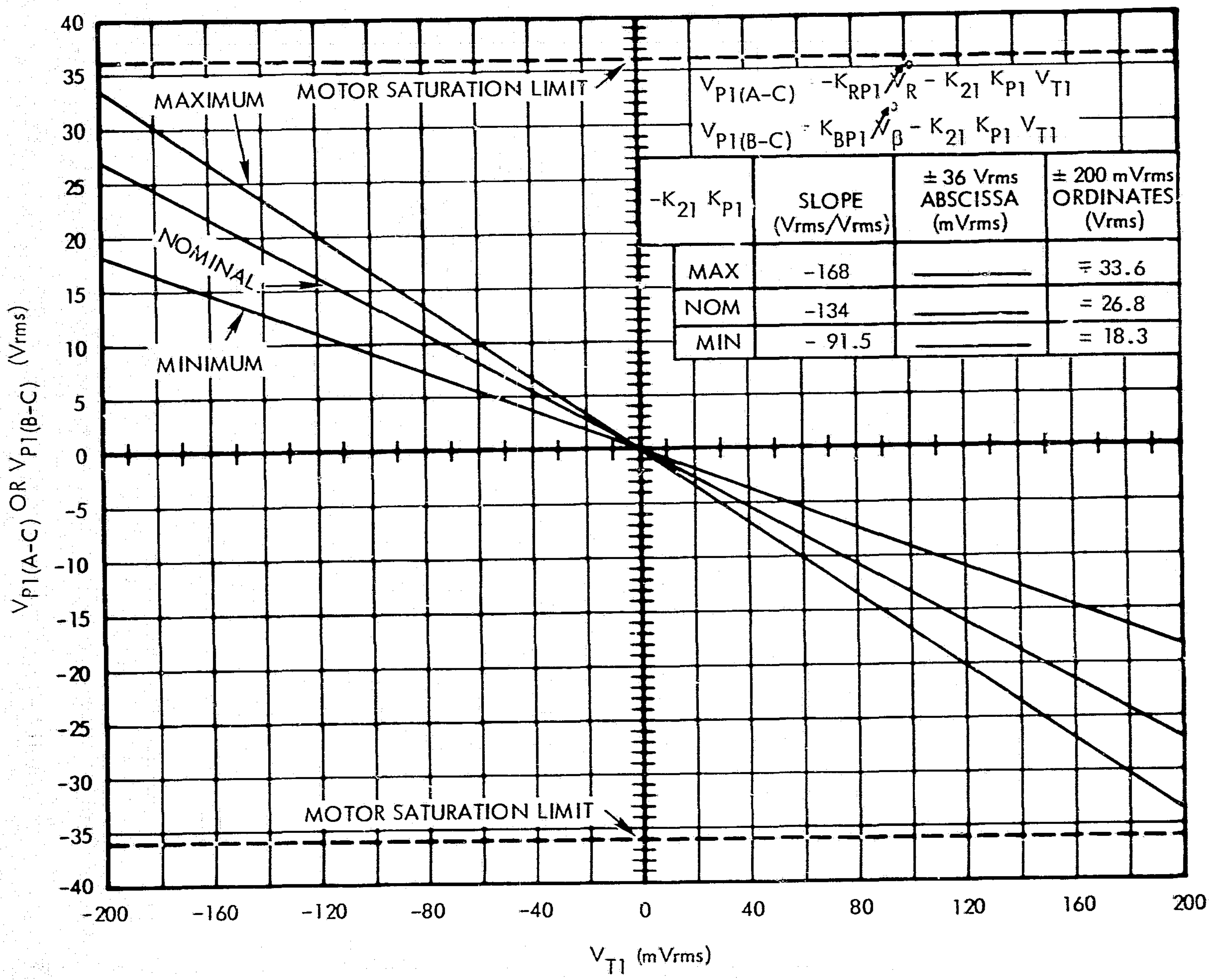

A-C or B-C Tracking Mode; A Axis Motor Drive Limits
as a Function of A Axis Tachometer Output
$V_{P1(A-C)}$ or $V_{P1(B-C)}$ Versus V_{T1} (Without Phase Shifts)

Figure 4-11

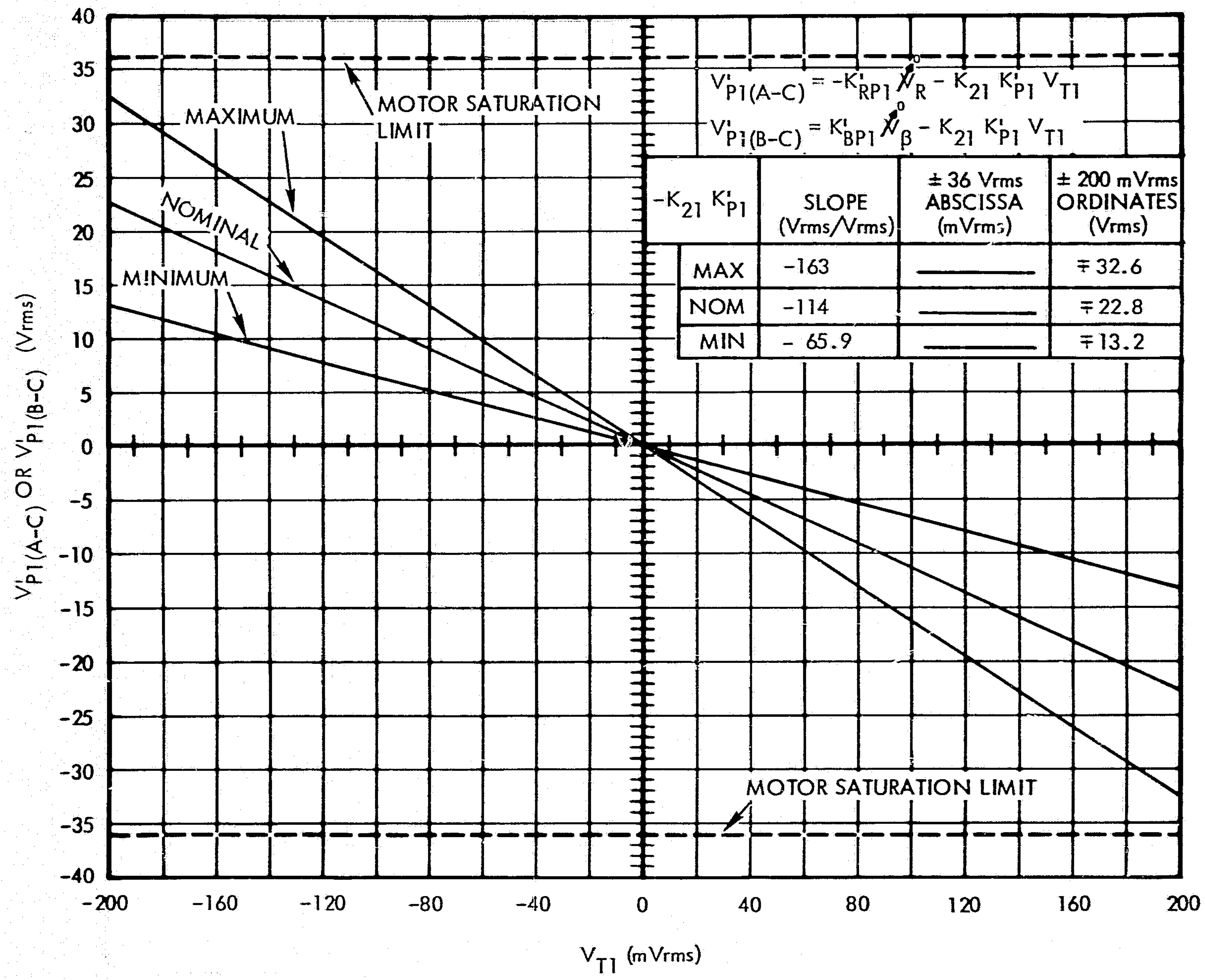

A-C or B-C Tracking Mode; A Axis Motor Drive Limits as a Function of A Axis Tachometer Output $V'_{P1(A-C)}$ or $V'_{P1(B-C)}$ Versus V_{T1} (With Phase Shifts)

Figure 4-12

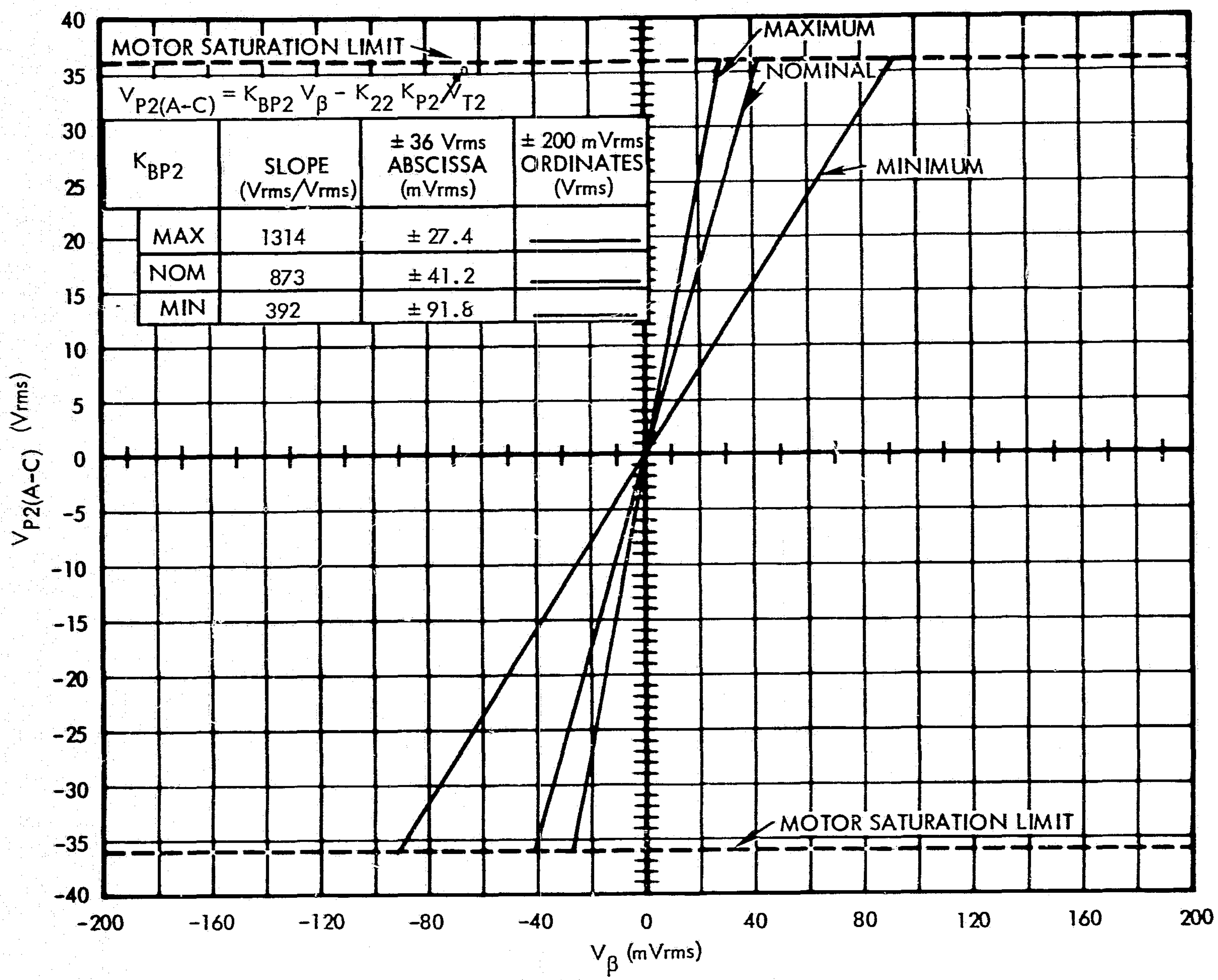

A-C Tracking Mode; B Axis Motor Drive Limits
as a Function of B Axis Induction Potentiometer (BIP) Output
$V_{P2(A-C)}$ Versus V_β (Without Phase Shifts)

Figure 4-13

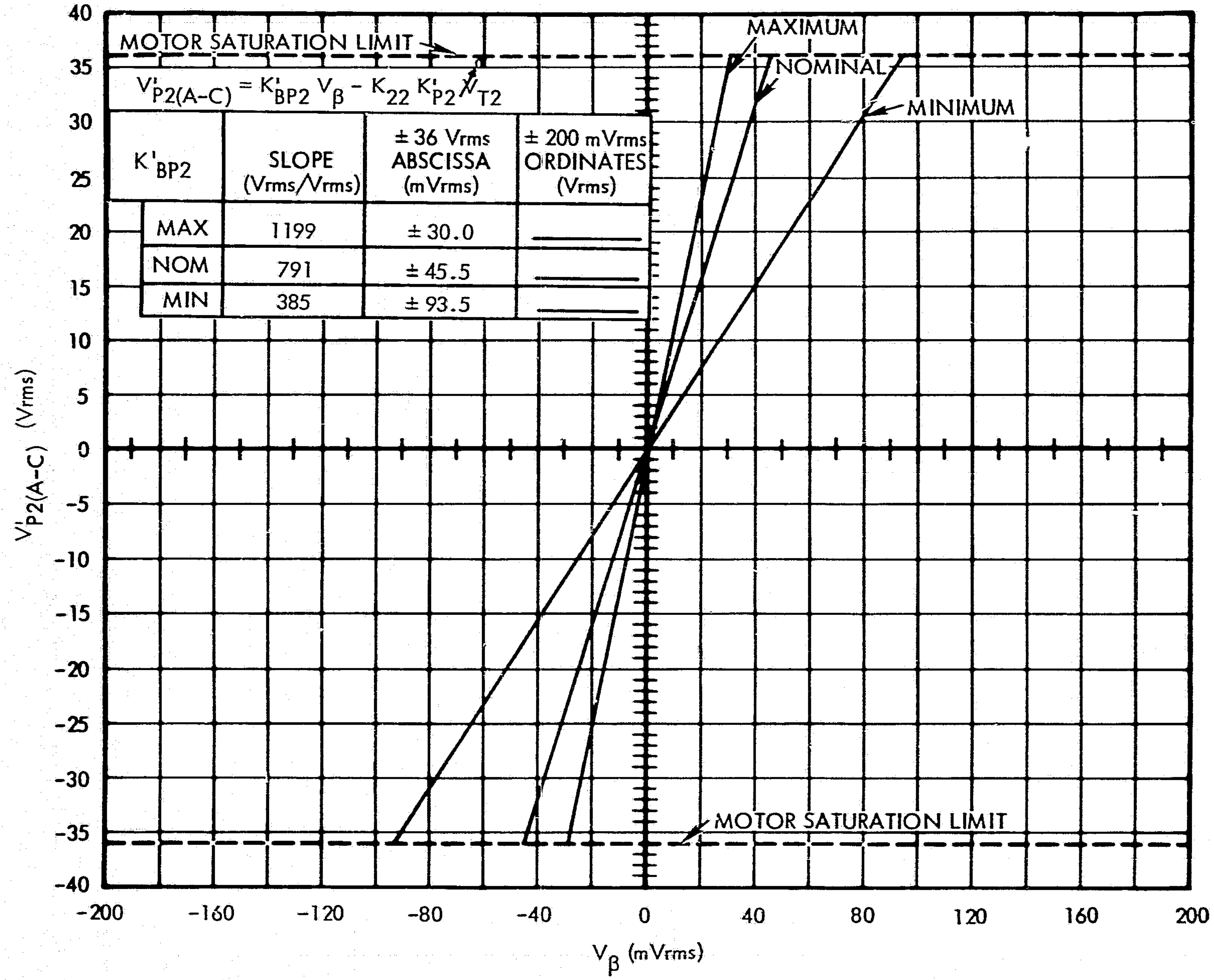

K'_{BP2}	SLOPE (Vrms/Vrms)	± 36 Vrms ABSCISSA (mVrms)	± 200 mVrms ORDINATES (Vrms)
MAX	1199	± 30.0	
NOM	791	± 45.5	
MIN	385	± 93.5	

A-C Tracking Mode; B Axis Motor Drive Limits
as a Function of B Axis Induction Potentiometer (BIP) Output
$V'_{P2(A-C)}$ Versus V_β (With Phase Shifts)

Figure 4-14

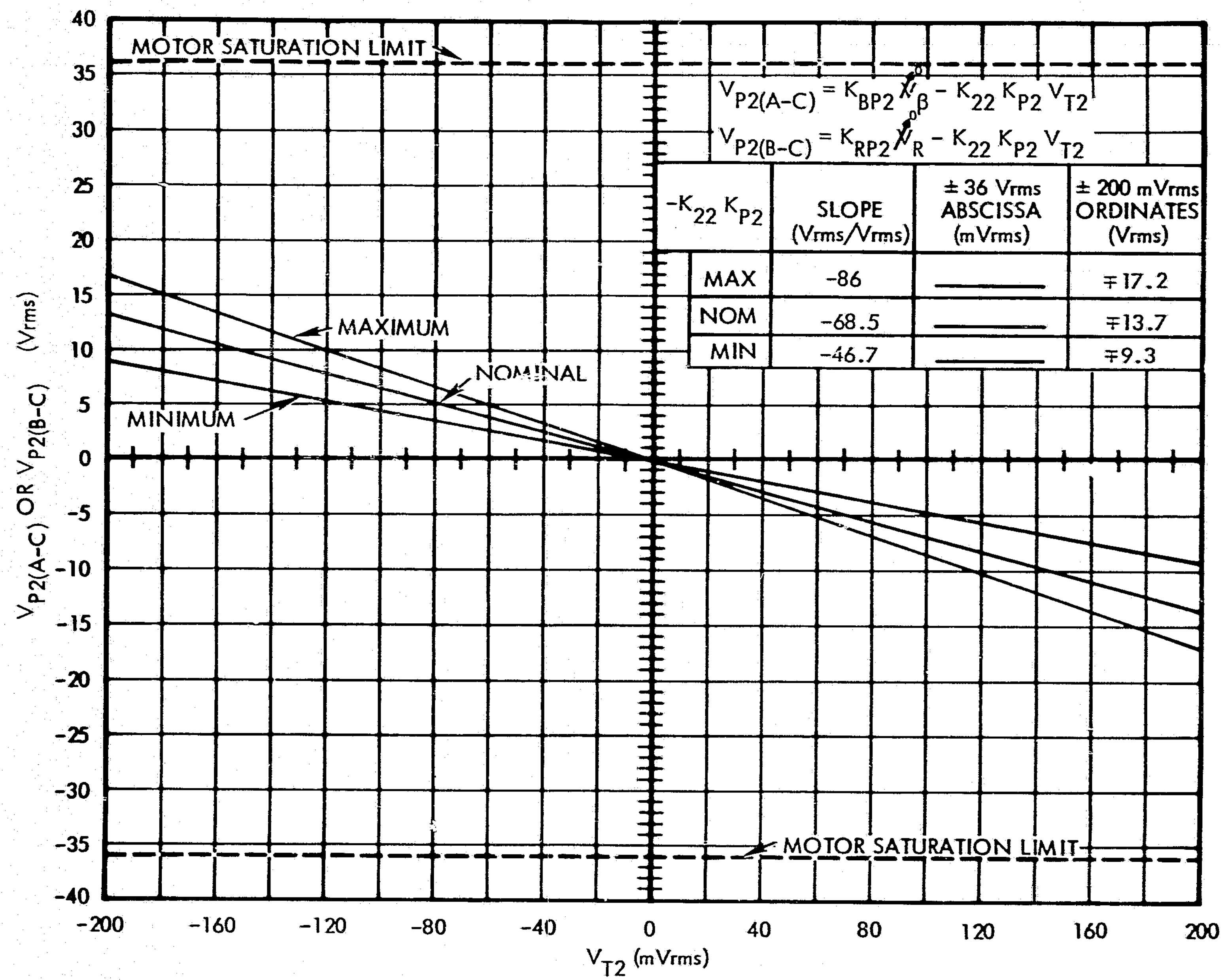

A-C or B-C Tracking Mode; B Axis Motor Drive Limits
as a Function of B Axis Tachometer Output
(Identical to Figure 4-19) $V_{P2(A-C)}$ or $V_{P2(B-C)}$ Versus V_{T2} (Without Phase Shifts)

Figure 4-15

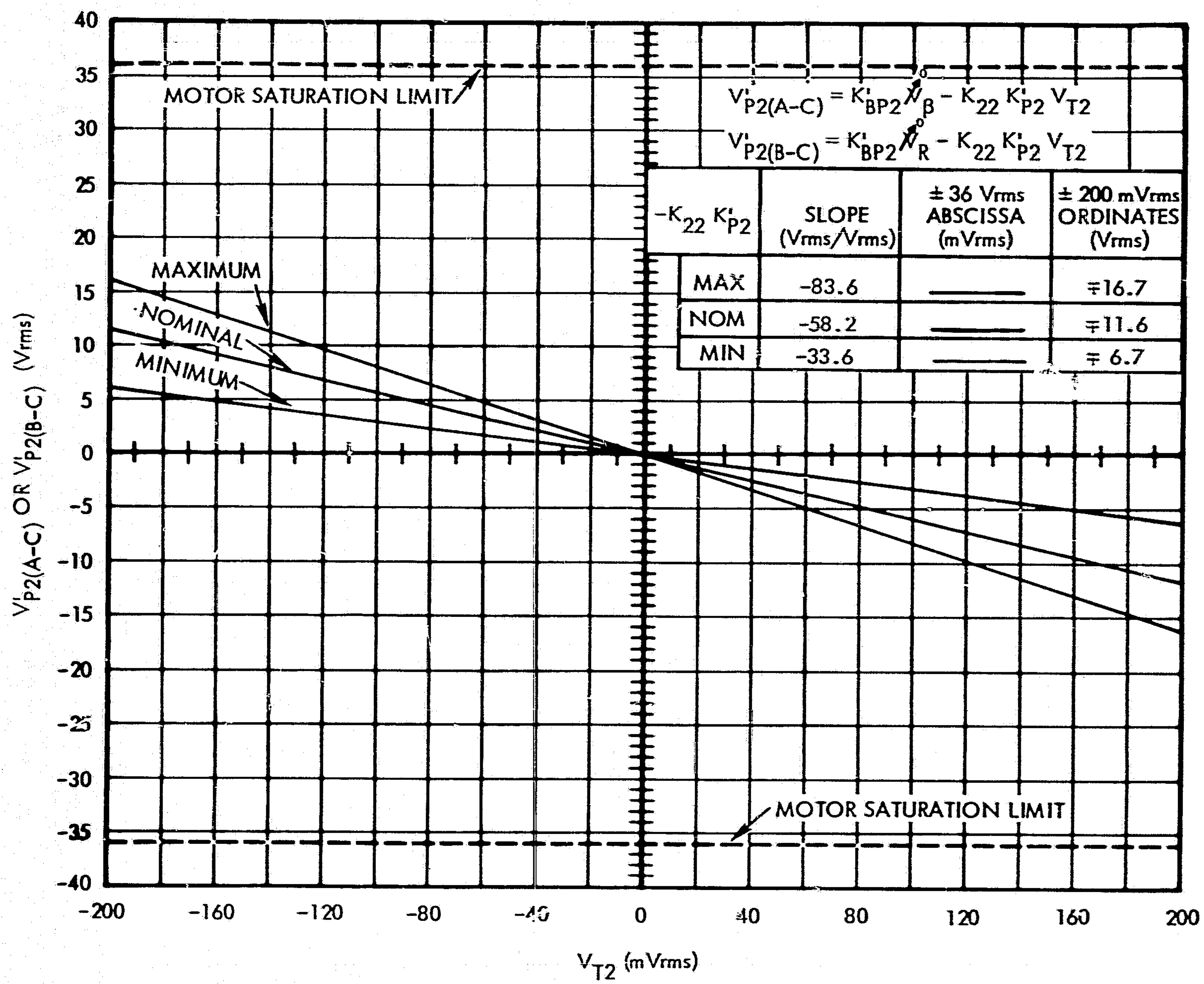

A-C or B-C Tracking Mode; B Axis Motor Drive Limits
as a Function of B Axis Tachometer Output
$V'_{P2(A-C)}$ or $V'_{P2(B-C)}$ Versus V_{T2} (With Phase Shifts)

(Identical to Figure 4-20)

Figure 4-16

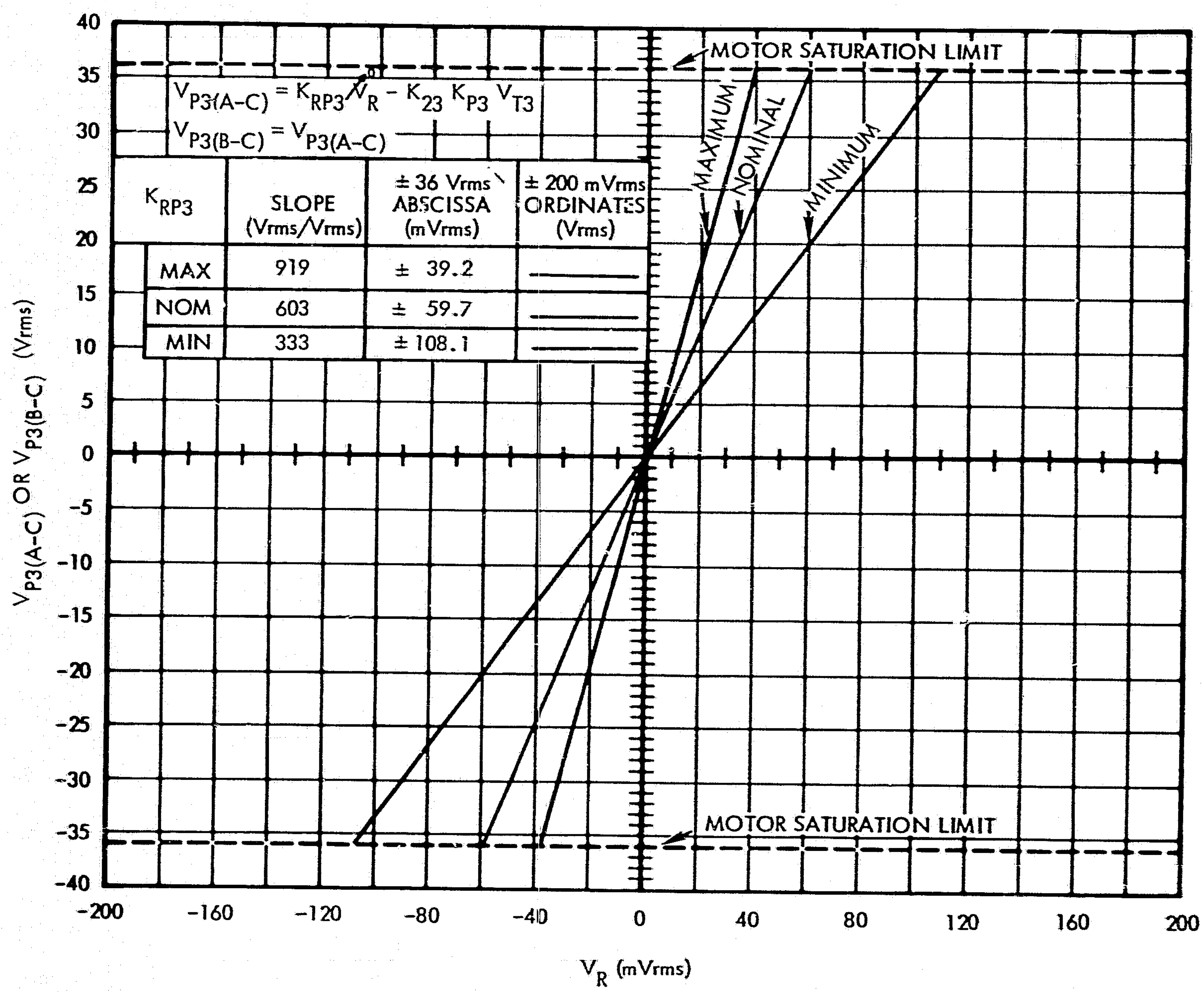

A-C or B-C Tracking Mode; C Axis Motor Drive Limits as a Function of Receiver Output $V_{P3(A-C)}$ or $V_{P3(B-C)}$ Versus V_R (Without Phase Shifts)

Figure 4-17

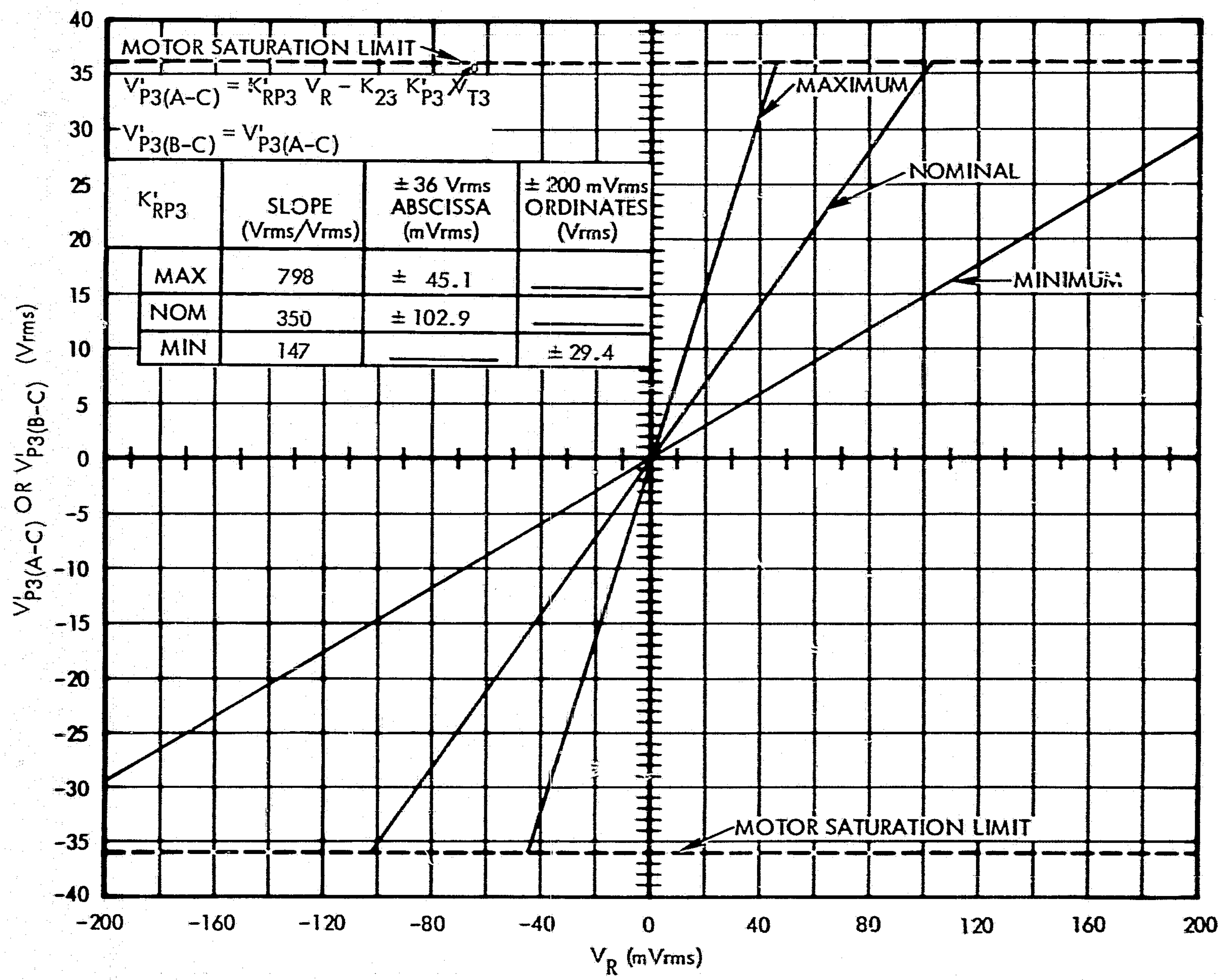

A-C or B-C Tracking Mode; C Axis Motor Drive Limits
as a Function of Receiver Output
$V'_{P3(A-C)}$ or $V'_{P3(B-C)}$ Versus V_R (With Phase Shifts)

Figure 4-18

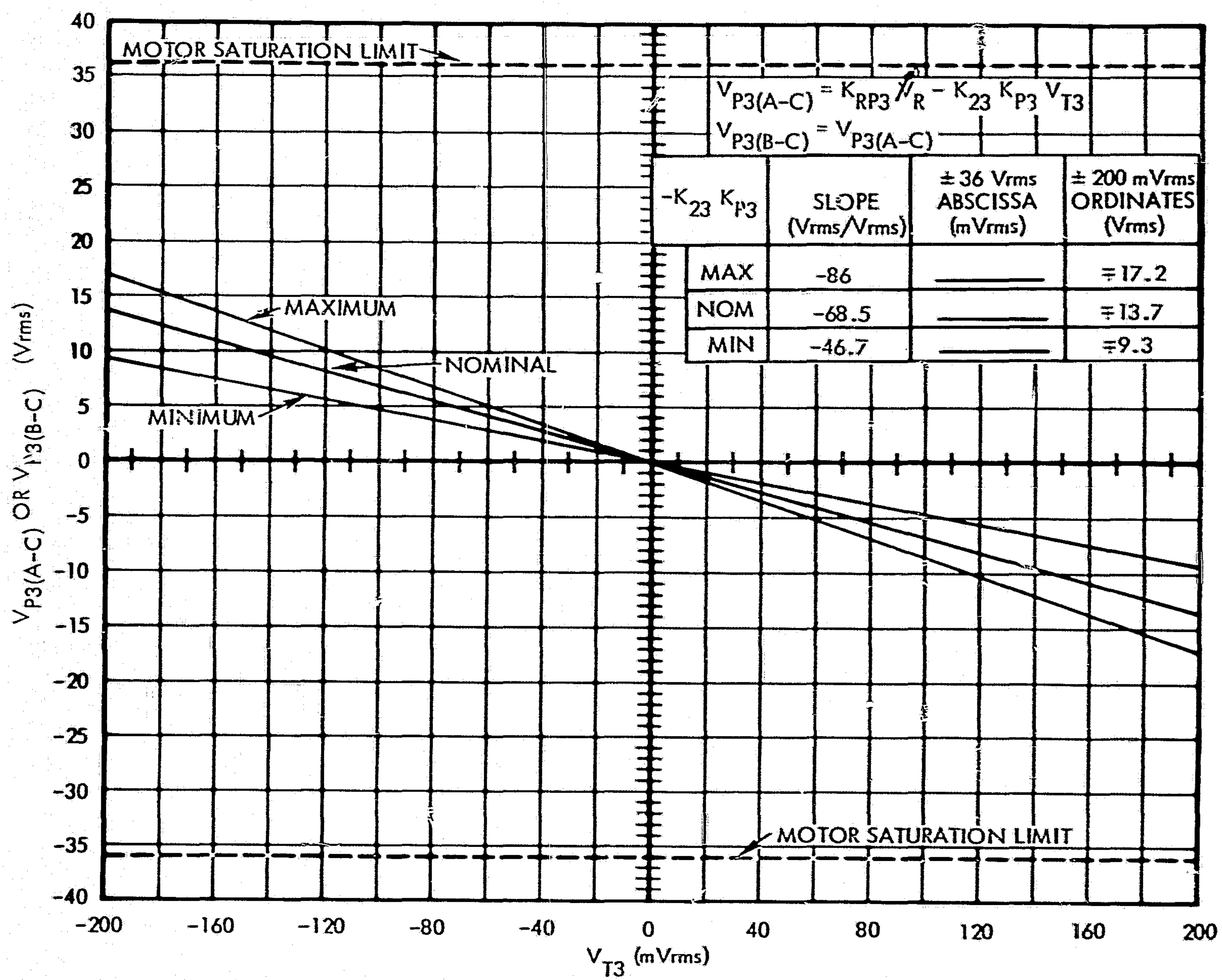

A-C or B-C Tracking Mode; C Axis Motor Drive Limits as a Function of C Axis Tachometer Output $V_{P3(A-C)}$ or $V_{P3(B-C)}$ Versus V_{T3} (Without Phase Shifts)

Figure 4-19

(Identical to Figure 4-15)

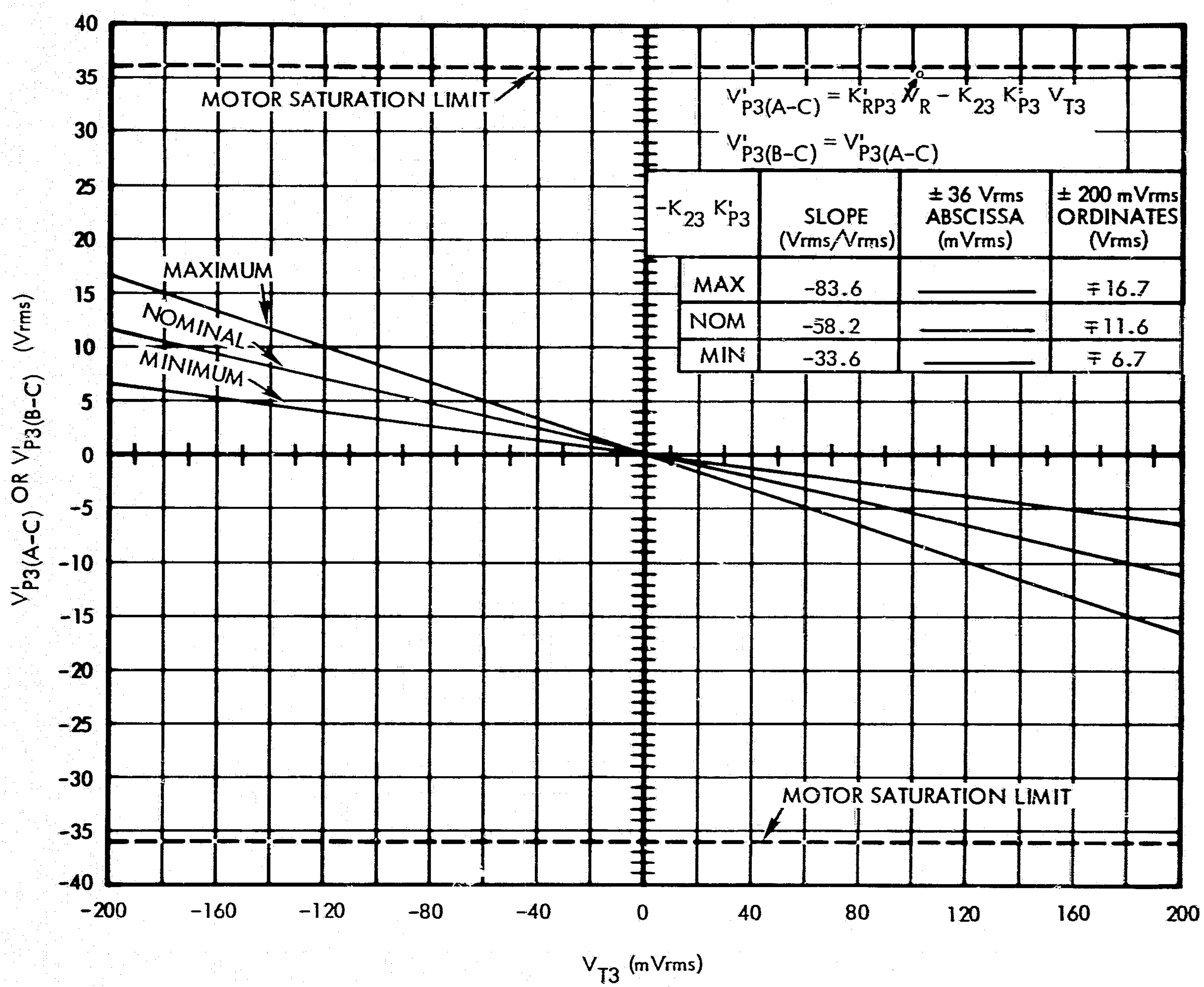

A-C or B-C Tracking Mode; C Axis Motor Drive Limits as a Function of C Axis Tachometer Output $V'_{P3(A-C)}$ or $V'_{P3(B-C)}$ Versus V_{T3} (With Phase Shifts)

Figure 4-20

(Identical to Figure 4-16)

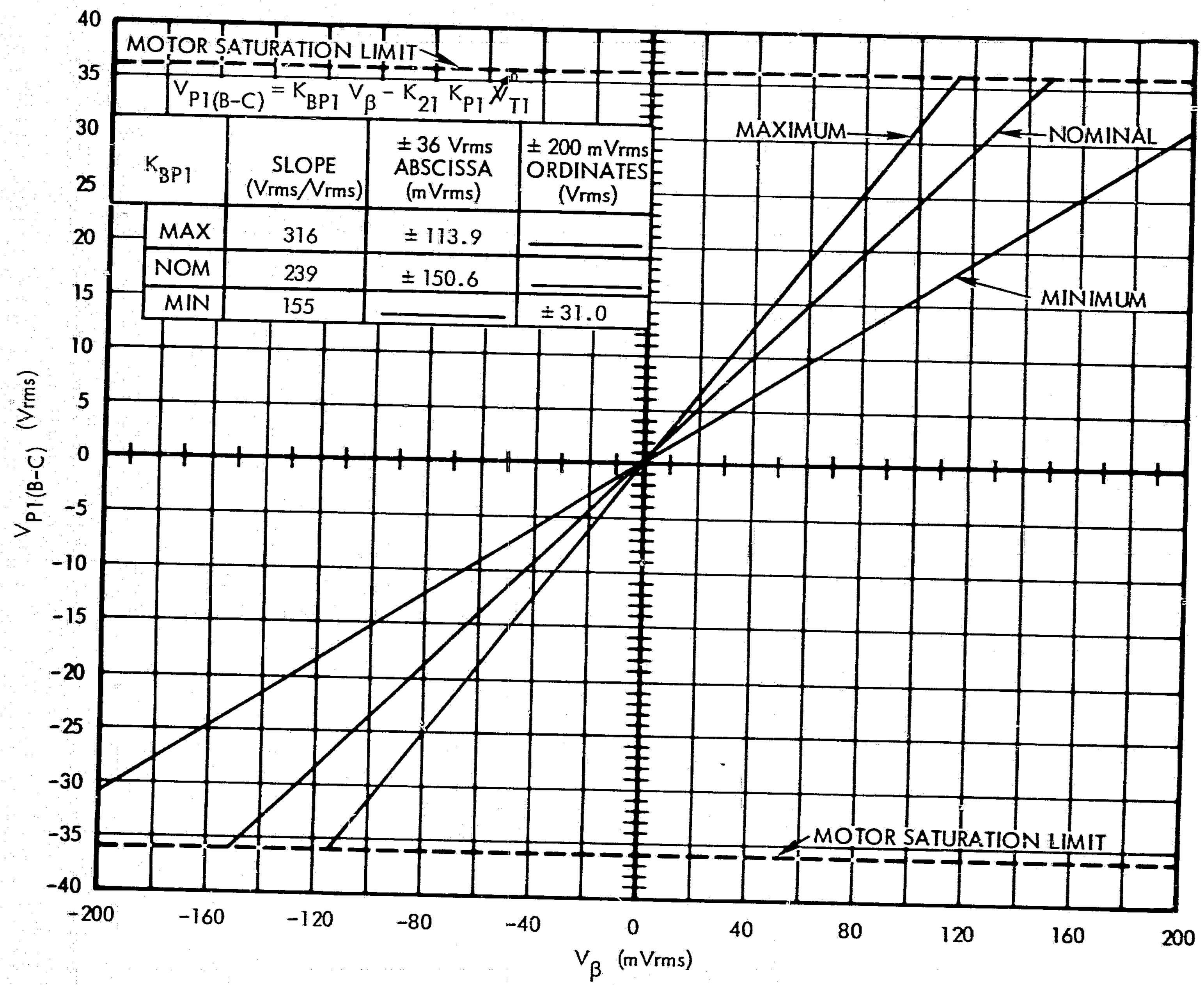

B-C Tracking Mode; A Axis Motor Drive Limits
as a Function of B Axis Induction Potentiometer (BIP) Output
$V_{P1(B-C)}$ Versus V_β (Without Phase Shifts)

Figure 4-21

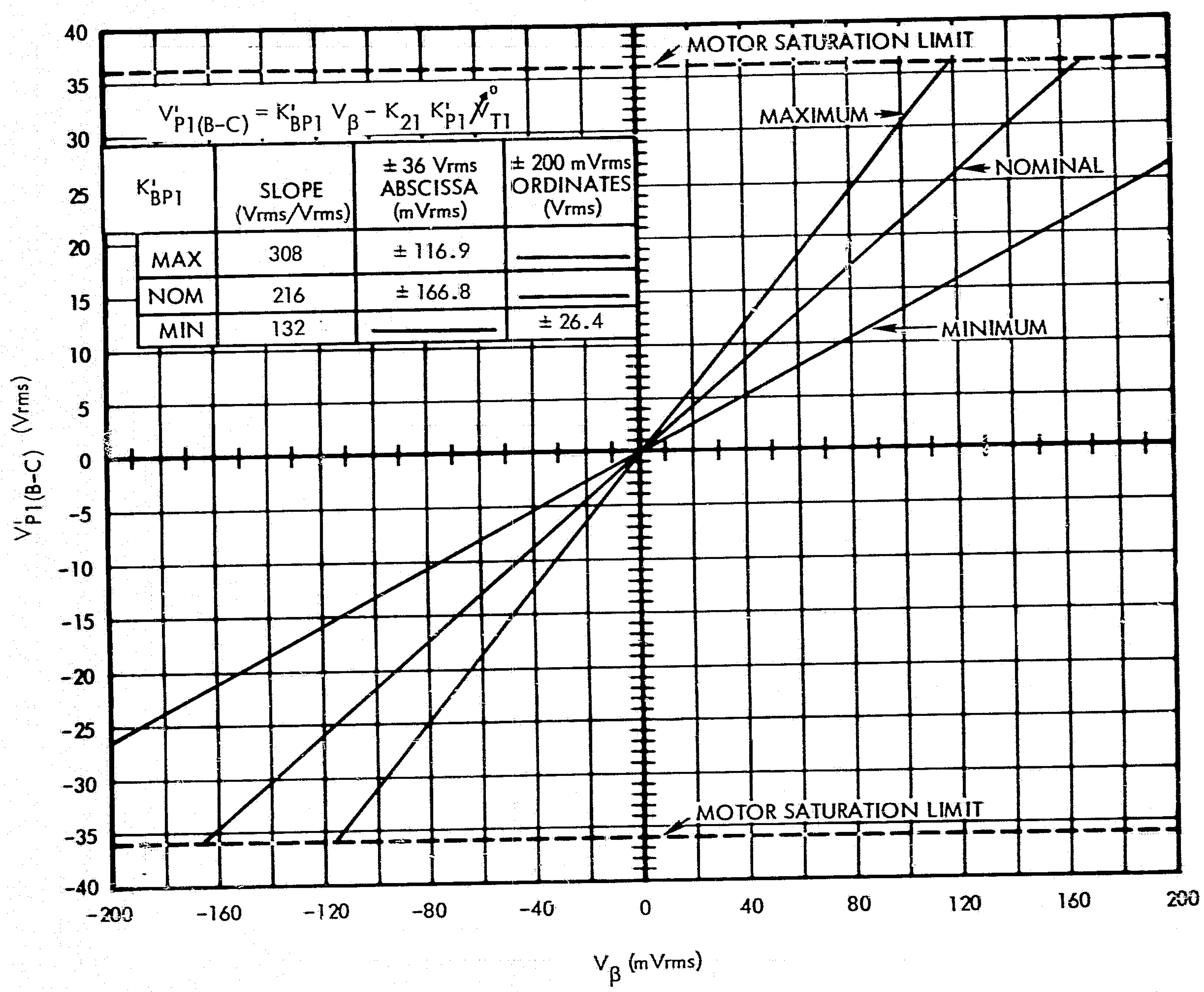

K'_{BP1}	SLOPE (Vrms/Vrms)	± 36 Vrms ABSCISSA (mVrms)	± 200 mVrms ORDINATES (Vrms)
MAX	308	± 116.9	———
NOM	216	± 166.8	———
MIN	132	———	± 26.4

B-C Tracking Mode; A Axis Motor Drive Limits
as a Function of B Axis Induction Potentiometer (BIP) Output
$V'_{P1(B-C)}$ Versus V_β (With Phase Shifts)

Figure 4-22

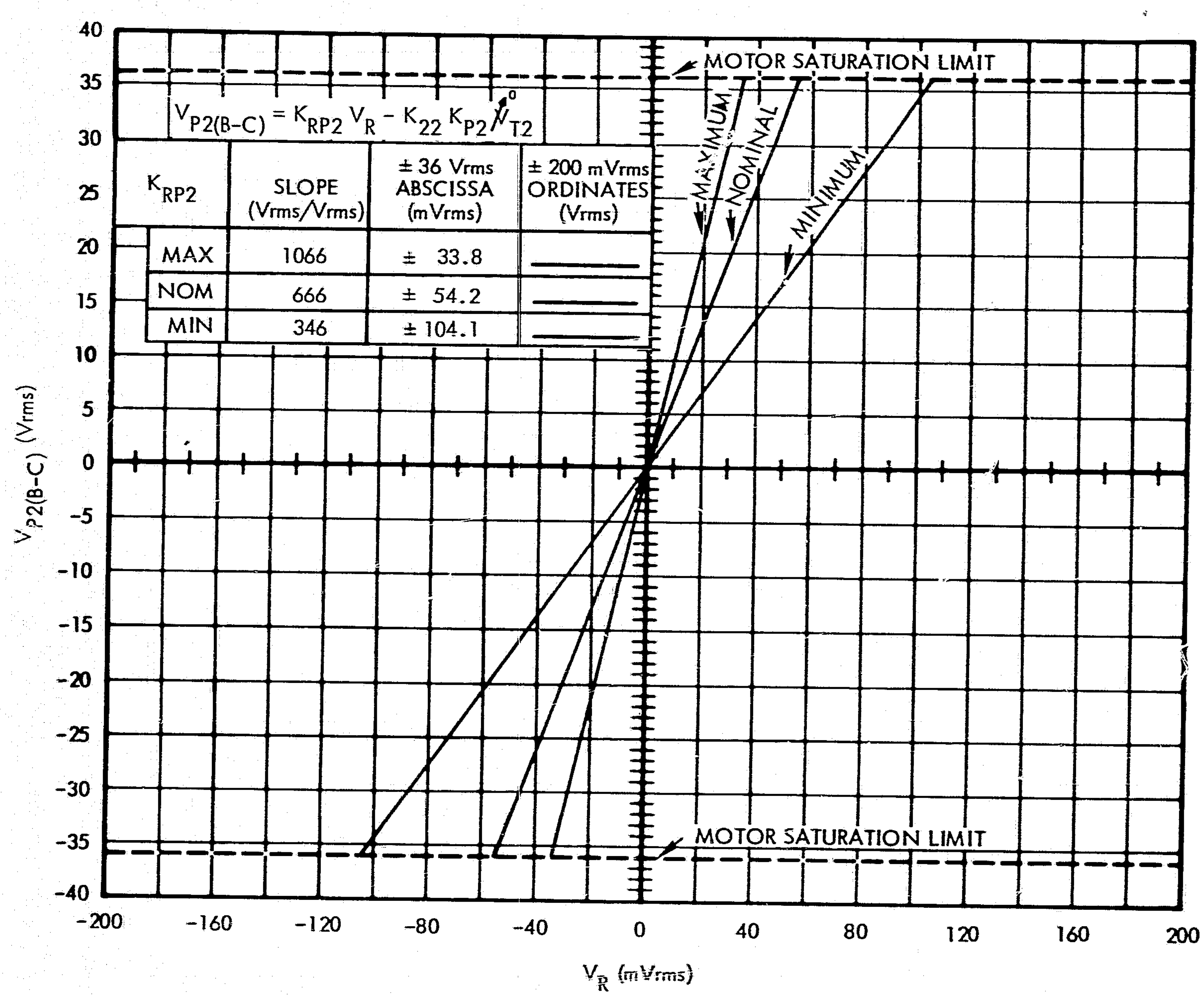

B-C Tracking Mode; B Axis Motor Drive Limits
as a Function of Receiver Output
$V_{P2(B-C)}$ Versus V_R (Without Phase Shifts)

Figure 4-23

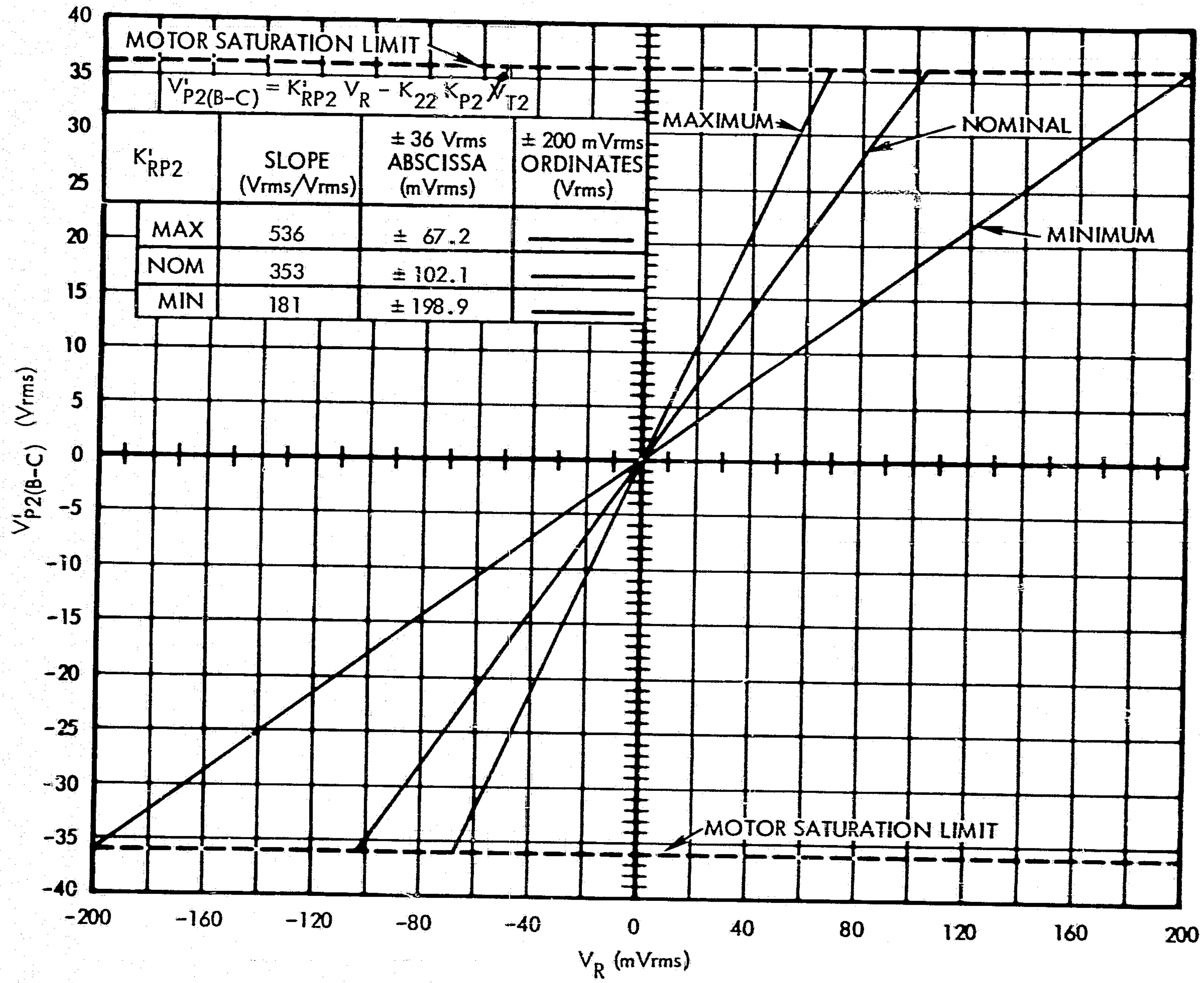

B-C Tracking Mode; B Axis Motor Drive Limits
as a Function of Receiver Output
$V'_{P2(B-C)}$ Versus V_R (With Phase Shifts)

Figure 4-24

Each graph in Figures 4-9 through 4-24 is plotted with ±36 Vrms maximum ordinate values (the motor saturation limit)* and ±200 millivolts rms maximum abscissa values (an arbitrarily chosen figure). Here, "+" is distinguished from "-" by a 180° phase difference in the 400 Hz signals. Since all graphs are plotted to the same scale, composite effects can be determined by graphically adding (e.g., by using a ruler or dividers) the appropriate values taken from the graphs.** For example, using the Figures 4-9 and 4-11 nominal curves, the A Axis power amplifier output $V_{P1(A-C)} \approx -8.2$ Vrms for a receiver output $V_R \approx 10$ mVrms (azimuth component only) and an A Axis tachometer output $V_{T1} \approx 10$ mVolts. If the antenna-receiver scale factor is taken as 1 Vrms/Deg and the tachometer scale factor is taken as 10^{-4} Vrms/Deg/Sec, then this A Axis power amplifier output $V_{P1(A-C)} \approx -8.2$ Vrms corresponds to an azimuth tracking error $\theta_a \approx 0.01$ deg and an A Axis motor velocity $\omega_{M1} \approx 100$ deg/sec.

Assuming worst-case input parameters ($K_A K_R = 1.62$ Vrms/Deg, $K_B K_{B2} = 0.215$ Vrms/Deg, and $K_T = 10^{-4}$ Vrms/Deg/Sec) and worst-case Electronics Assembly parameters ($K'_{RP} = 798$ Vrms/Vrms, $K'_{BP} = 1199$ Vrms/Vrms, and $K_2 K'_P = 163$ Vrms/Vrms), the motors can be made to saturate with the linear model assumed here with (separate) azimuth or elevation tracking errors of about ±0.03 deg, B Axis angles of about ±0.15 deg, or motor velocities of about ±2000 deg/sec (67 RPM). Using nominal parameters ($K_A K_R = 1.13$ Vrms/Deg, $K_B K_{B1} = 0.09$ Vrms/Deg, $K_T = 8 \times 10^{-5}$ Vrms/Deg/Sec, $K'_{RP} = 35.5$ Vrms/Vrms, $K'_{BP} = 503$ Vrms/Vrms, and $K_2 K'_P = 76.8$ Vrms/Vrms), these limits become about ±0.09 deg tracking error, about ±0.8 deg β angle, or about ±6000 deg/sec (200 RPM) motor velocity.

These approximate limits work as an "uncertainty principle" in the sense that if one of the factors reaches its limit, the other two factors must be zero. If two or all three factors are non-zero, the limits for each must be reduced accordingly.

* The motors saturate at ±0.4 in-oz output torques for power amplifier outputs of ±36 Vrms.

** An alternative to this data presentation could have been a family of curves of, for example, $V_{P1(A-C)}$ versus V_R for selected values of V_{T1}. However, such a format is of questionable value, since testing of the Electronics Assembly as an entity can be accomplished with all but one input zero, as documented in Figures 4-9 through 4-24.

5.0 VOLUME I SUMMARY AND CONCLUSIONS

Volume I documents the linear, small signal characteristics of the CSM High Gain Antenna Tracking System Electronics Assembly and estimates the nominal and absolute worst-case limits of the small signal Electronics Assembly input/output transfer functions. Using the Table 2-1 parameter data supplied by Autonetics (Reference 2), the transfer function characteristics (Section 4.0) are determined, based on a linear model of the Electronics Assembly (Figure 3-1). Due to motor saturation and other system non-linearities, the use of this linear model is limited to small tracking errors (up to about ±0.1 degrees or less), small B Axis angles (up to about $\beta = \pm 1$ degree or less), and relatively small motor angular velocities (up to about ±200 RPM or less).

Expected Small Signal Electronics Assembly receiver-output-to-servo-motor-drive-input DC gains range between 333 Vrms/Vrms minimum to 1066 Vrms/Vrms maximum over the range 77°F to 200°F, for signals where phase shift effects have been ignored. When phase shift effects are included*, these equivalent gains range between 131 Vrms/Vrms and 798 Vrms/Vrms. The expected B Axis Induction Potentiometer (BIP) output-to-servo-motor-drive-input DC gains vary from 155 Vrms/Vrms minimum to 1314 Vrms/Vrms maximum, without phase shift considerations, and from 132 Vrms/Vrms to 1199 Vrms/Vrms, with phase shifts included. The expected tachometer-output-to-servo-motor-drive-input DC gains range between 46.7 Vrms/Vrms and 168 Vrms/Vrms when phase shifts are ignored and from 33.6 Vrms/Vrms to 163 Vrms/Vrms with phase shifts**. The net servo motor drive inputs can be determined by adding the separate effects.

The frequency compensation characteristics of the Electronics Assembly cause the above receiver-to-motor gains to be multiplied by unity at 0 Hz perturbation frequency, by an average of ~ 0.85 at 0.1 Hz, by ~ 0.25 at 1 Hz, and by ~ 0.15 at 10 Hz. Complete frequency characteristics are given in Paragraph 4-4.

* The servo motors use only that portion of the drive signals which is in phase-quadrature (90° out-of-phase) with the 400 Hz reference.

** These latter values do not include the effects of phase shifts within the tachometers themselves.

Since Electronics Assembly Interchangeability is a system considera whether or not the Electronics Assembly is interchangeable cannot be dete, mined solely from the data presented in this report. Neither can this data be interpreted as specifications of limits within which the Electronics Assembly must be tested to ensure interchangeability. However, the results of this report can be used to predict the performance of the Electronics Assembly as it is presently configured.

This and other analyses of the Electronics Assembly will be combined with analyses of the other portions of the Tracking System to show whether the system can perform satisfactorily. A successful overall system analysis of this type would then indicate that the Electronics Assembly is interchangeable without further modification and that the data presented herein is acceptable as test limit specifications.

APPENDIX A

The data presented in this report was partially generated using three digital computer programs: AFZHGA, HC003B, and TRWPLT.

Program AFZHGA ("High Gain Antenna") is an on-line remote-terminal time-sharing program prepared by the author in the RUSH programming language; it is run on a remote terminal at TRW/Houston. This program receives as input the Autonetics data given in Table 2-1 of this report. The output of this program, as used in this report, is given in Tables 4-1 and 4-2. As such, AFZHGA is a mechanization of the formulas given in Tables 4-1 and 4-2.

Program HC003B is a TRW/Houston Computation Center (HCC) Univac 1108 version of a TRW Redondo Beach program called "Linear System Dynamics Program", or "LSD" for short. LSD has many options, including Eigen-Value matrix solutions, Frequency Response calculations, Root Locus calculations, and Transient Response (inverse LaPlace transform) calculations. All computation options except Eigen-Value have sub-options of graphical plots (either Calcomp or 4020 microfilm) via Program TRWPLT. This report uses the LSD Frequency Response with plot option, where the $G_{C1}(s)$ and $G_{C3}(s)$ transfer functions (Paragraph 4.4) are input as s-plane open-loop poles, zeros, and gains. The tabulated computer output, as used in this report, is given in Table 4-5. The plot option generates a data tape for Program TRWPLT.

Program TRWPLT is a TRW HCC Univac 1108 Generalized Plot Program which is thoroughly described in Reference (4). Its inputs are a data tape (in this case generated by LSD) and a deck of control cards which specify how the data tape is to be processed. The resulting 4020 microfilm plots for this report are shown in Figures 4-1 through 4-8.

REFERENCES

1. TRW Report 1176-H013-TO-00, LM and CSM S-Band Antenna Tracking Studies, Task E-53C, Engineering Report, Interchangeability Study - Data Acquisition Status Report, Chan, Fogel, Osborn, and Robinson, 9 August 1968.

2. Autonetics Report TR-1819/301, Apollo CSM High Gain Antenna, Volume I, Circuit and System Analysis, G. B. Way, 16 August 1968.

3. Dalmo Victor Report R-3028-4751, Development Testing of Redesigned Electronics for XDV-7 and Subsequent Apollo High Gain Antennas, Lloyd, Eng, and Walker, 28 June 1968.

4. TRW HCC Report 3141.20-10, TRWPLT Generalized Plot Program, Input Manual, C. E. Coflin, July 1968.